High-Resolution spectroscopy and analysis of the fundamental modes of 28 Si F 4 . Accurate experimental determination of the Si – F bond length

V. Boudon, C. Richard, L. Manceron

High-Resolution spectroscopy and analysis of the fundamental modes of $^{28}SiF_4$. Accurate experimental determination of the Si−F bond length.

V. Boudon[a,*], C. Richard[a], L. Manceron[b,c]

[a] *Laboratoire Interdisciplinaire Carnot de Bourgogne, UMR 6303 CNRS - Université Bourgogne Franche-Comté, 9 Av. A. Savary, BP 47870, F-21078 Dijon Cedex, France*
[b] *Synchrotron SOLEIL, AILES Beamline, L'Orme des Merisiers, St-Aubin BP48, 91192 Cedex, France*
[c] *MONARIS, UMR 8233, Université Pierre et Marie Curie, 4 Place Jussieu, case 49, F-75252 Paris Cedex 05, France*

Abstract

Silicon tetrafluoride (SiF_4) is a trace component of volcanic gases and is gaining industrial importance. However, a better knowledge of spectroscopic parameters is needed for this molecule in order to derive accurate concentrations. Following a previous reinvestigation of the ν_3 and ν_4 fundamentals [*J. Quant. Spectrosc. Radiat. Transfer* **260** (2021) 107474], we have undertaken an extensive high-resolution study of its infrared absorption bands. We present here an update of this study. It features the recording of new far-infrared spectra, taking advantage of synchrotron radiation, and a global fit giving a consistent parameter set for the ground and fundamental states of $^{28}SiF_4$, now including the $v_1 = 1$ and $v_2 = 1$ states, by adding to the global analysis the newly measured ν_2, $\nu_1 - \nu_4$, and $\nu_4 - \nu_2$ bands near 264, 412, and 125 cm^{-1}, respectively. Nearly 20 000 assigned lines pertaining to seven distinct rovibrational bands were fitted with an excellent accuracy (global standard deviation of 0.296). This allows us to obtain an accurate experimental value for the Si−F bond length, $r_e(SiF_4) = 1.5516985(30)$ Å. Some new band intensity estimates allow us to update our SiF_4 calculated spectroscopic database.

Keywords:
Silicon tetrafluoride, High-resolution infrared spectroscopy, Tensorial formalism, Line positions, Bond length, Integrated band intensities

1. Introduction

Silicon tetrafluoride (SiF_4) is the most stable of silicon halides and is thus used in several industrial processes in the electronic and optical industry as a precursor for various Si-based materials [1]. A renewed interest in the spectroscopic methods applied to this molecule has

*Corresponding author
Email address: Vincent.Boudon@u-bourgogne.fr (V. Boudon)

been spurred by two different domains. It is produced in volcanic activity [2, 3, 4, 5, 6, 7] and used as a marker of deep magma ingress in some volcanic chambers [8, 9], therefore detected by remote infrared (IR) spectroscopic methods. Secondly, the necessity of improving some silicon physical properties for the future development of spintronics imposes drastic purity constraints as well as a need to prepare isotopically pure $^{28}SiF_4$ for material synthesis [10]. Again, monitoring methods using IR spectroscopy will be useful in these developments. If many low resolution IR and Raman studies have located all SiF_4 fundamentals [11], the knowledge of its rovibrational spectroscopy was however restricted until a recent date to a few IR diode high resolution (HR) studies on selected portions of the strong ν_3 band region [12, 13], followed by double resonance experiment to obtain precious information on the ground state spectroscopic constants [14]. Lately, the other IR-active fundamental (the ν_4 bending mode near 388.4 cm^{-1}) was observed at HR using synchrotron radiation (SR) [15].

In addition to the industrial and geological applications mentioned above, the study of the structural and spectroscopic properties of SiF_4 is an interesting matter in itself, as the quantum chemical treatment of molecules with second-row atoms stills requires some degree of semi-empirical corrections using experimentally determined properties. Two important milestones in this respect are the equilibrium structure and the rovibrational level positions and IR intensities. Regarding the structure, as the molecule is a spherical top with T_d symmetry, the equilibrium structure depends on a single parameter, the equilibrium bond length, r_e. Following two electron diffraction studies giving two different estimates: r_e = 1.555(2) [16] and 1.552(2) Å [17], several spectroscopic studies improved the situation. Since observation of rotational lines in the vibrational ground state (GS) cannot be made in direct absorption, Jörissen *et al.* [14] reported a B_0 GS value based on their double resonance experiment on some 182 lines. This resulted in an r_0 value estimated at 1.55982(17) Å. Yet, vibrational corrections must still be made to obtain an estimate of the equilibrium bond length. J. Breidung *et al.* devoted next a study to test the different approximate methods for deducing the equilibrium structure [18]. Depending on the method chosen, Ref. [18] narrowed substantially the range for possible r_e values to 1.5524(8) Å. Nevertheless, there is still room for improvement if one can observe rotationally resolved spectra for all four SiF_4 fundamentals in order to carry out a more exact vibrational correction on B_0 to access B_e and thus r_e.

The advent of improved instrumentation to couple SR [19, 20] to HR interferometry, long path cryogenic cells [21] and improved detectors has opened the way to the observation of rovibrationally resolved very weak bands in the mid to far infrared regions (these being either first-order forbidden fundamentals or weak difference bands involving IR-forbidden states [22, 23, 24]). This study is thus devoted to the observation and analysis of weak bands involving the ν_1 and ν_2 fundamentals or, more generally, the $v_1 = 1$ or $v_2 = 1$ states. Secondly, an improved estimate of the equilibrium bond length is proposed.

This paper is organized as follows: Section 2 below presents the spectrum measurements, Section 3 details the theoretical model used, Section 4 gives our results for spectrum analyses, equilibrium bond length and band intensity estimates. Finally, Section 5 presents the TFSiCaSDa (Tetra-Fluoro Silane Calculated Spectroscopic Database [25]) database update.

2. Experiment

Because of the weakness of the difference bands or multi quanta transitions, a long optical path length at low temperature was required. In the far and mid- IR, several high resolution spectra were recorded on the AILES Beamline at Synchrotron SOLEIL (Saint-Aubin, France). The Synchrotron light source was coupled to the Bruker 125HR interferometer [19, 20] using the AILES cryogenic long path cell regulated at 163 K temperature along the entire optical path, set up to 93 m. This setup has been fully described elsewhere [21]. For these spectra, the SR from the SOLEIL facility (500 mA in 316 bunches mode) was used as a source, without limitation of the interferometer entrance aperture.

For the very weak difference bands analysed in this study, a spectrum with a gas pressure of 14.9 mbar of SiF_4 (Orano, France, better than 99.99 % purity) was recorded at 0.002 cm^{-1} resolution in the 60–800 cm^{-1} region, using boxcar apodization, 5.06 cm/s scanner velocity, a 6 μm Si-Mylar beamsplitter and a 4K-cooled Si composite bolometer with a 1.5 ms rise time and a cold, 700 cm^{-1} low-pass filter. 576 interferograms were averaged in a total recording time of about 38 hours and processed against a background of the empty cell taken at the same 163 K temperature and 0.01 cm^{-1} resolution. Another spectrum was taken at a lower pressure (0.44 mb) to avoid saturation for the ν_2 band region. A third spectrum was recorded at 0.002 cm^{-1} resolution using a Ge-KBr beamsplitter and a home-made high sensitivity 4 K-cooled HgCdTe detector [26] using the same 93 m length (see Table 1). Spectra were zero-filled, corrected for channelling effects and calibrated using well-known water and carbon dioxide or carbonyl sulphide rovibrational lines [27] with a standard deviation of about 3×10^{-4} cm^{-1}.

3. Theoretical model

3.1. Vibrational polyads

As already mentioned in our previous work [15], silicon tetrafluoride is a tetrahedral spherical top molecule with T_d point group symmetry at equilibrium and possesses four normal modes of vibration: ν_1 (non-degenerate, A_1 symmetry 800.7 cm^{-1}), ν_2 (doubly degenerate, E symmetry, 264.2 cm^{-1}), ν_3 and ν_4 (triply degenerate, F_2 symmetry, 1031.5 and 388.4 cm^{-1}, respectively). The wavenumbers of these modes are such that the molecule exhibits a nicely defined vibrational structure, with polyads every *ca.* 130 cm^{-1}. More precisely, a vibrational level (v_1, v_2, v_3, v_4) pertains to polyad P_k if

$$k = 6v_1 + 2v_2 + 8v_3 + 3v_4. \tag{1}$$

In this scheme, there is no polyad number 1. The ground state (GS) is the vibrational level $(0, 0, 0, 0)$, and constitutes is polyad P_0, then level $v_2 = 1$ $(0, 1, 0, 0)$ constitutes polyad P_2, *etc.* Figure 2 schematically displays these polyads. It should be noticed that, along with methane (CH_4) [28, 29, 30], silicon tetrafluoride is one of the very few spherical-top molecules with such a well-defined polyad structure.

3.2. Effective Hamiltonian operator

Due to the high symmetry of the molecule, we use the tensorial formalism and group theory methods developed in the Dijon group [31, 32, 33]. Let us just recall briefly the principles of this model.

We are here considering an XY_4 molecule for which the vibrational levels can be grouped into a series of polyads named P_k with $k = 0, \ldots, n$, $P_{k=0}$ being the ground state (GS). The Hamiltonian operator is written as follows (assuming that some perturbative treatment such as a contact transformation [34, 35, 31] has been performed to eliminate inter-polyad interactions):

$$\mathcal{H} = \mathcal{H}_{\{P_0 \equiv GS\}} + \mathcal{H}_{\{P_1\}} + \ldots + \mathcal{H}_{\{P_k\}} + \ldots + \mathcal{H}_{\{P_{n-1}\}} + \mathcal{H}_{\{P_n\}}, \tag{2}$$

where the different $\mathcal{H}_{\{P_k\}}$ terms are expressed in the following form:

$$\mathcal{H}_{\{P_k\}} = \sum_{\text{all indexes}} t^{\Omega(K,n\Gamma)\Gamma_v\Gamma'_v}_{\{s\}\{s'\}} \beta \left[{}^{\varepsilon}V^{\Omega_v(\Gamma_v\Gamma'_v)\Gamma}_{\{s\}\{s'\}} \otimes R^{\Omega(K,n\Gamma)} \right]^{(A_1)}. \tag{3}$$

In this equation, the $t^{\Omega(K,n\Gamma)\Gamma v\Gamma' v}_{\{s\}\{s'\}}$ are the parameters to be determined, while ${}^{\varepsilon}V^{\Omega_v(\Gamma_v\Gamma'_v)\Gamma}_{\{s\}\{s'\}}$ and $\mathrm{R}^{\Omega(K,n\Gamma)}$ are vibrational and rotational operators, respectively. For each term, Ω_v and Ω represent the degree in elementary vibrational operators (creation a^+ and annihilation a operators), and rotational operators (components J_x, J_y and J_z of the angular momentum), respectively. β is a factor that allows the scalar terms (terms with $\Gamma = A_1$, the totally symmetric irreducible representation of T_d) to match the "usual" contributions like $B_0 J^2$, *etc*. The order of each individual term is defined as $\Omega + \Omega_v - 2$. We then deal with effective Hamiltonians which are obtained, for a given polyad P_k, by the projection of H on the P_n Hilbert subspace:

$$\begin{aligned} \widetilde{H}^{<P_n>} &= P^{<P_n>} \mathcal{H} P^{<P_n>} \\ &= H^{<P_n>}_{\{\mathrm{GS}\}} + H^{<P_n>}_{\{P_1\}} + \ldots + H^{<P_n>}_{\{P_k\}} + \ldots + H^{<P_n>}_{\{P_{n-1}\}} + H^{<P_n>}_{\{P_n\}}. \end{aligned} \tag{4}$$

In the present study, we will use data from the transitions indicated in red on Figure 2. We thus use the following effective Hamiltonians:

- The ground state effective Hamiltonian (polyad P_0),

$$\widetilde{H}^{<\mathrm{P_0}>} = H^{<\mathrm{P_0}>}_{\{\mathrm{P_0}\}}. \tag{5}$$

- The ν_2 bending fundamental effective Hamiltonian (polyad P_2),

$$\widetilde{H}^{<P_2>} = H^{<P_2>}_{\{\mathrm{P_0}\}} + H^{<P_2>}_{\{P_2\}}. \tag{6}$$

- The ν_4 bending fundamental effective Hamiltonian (polyad P_3),

$$\widetilde{H}^{<P_3>} = H^{<P_3>}_{\{\mathrm{P_0}\}} + H^{<P_3>}_{\{P_2\}} + H^{<P_3>}_{\{P_3\}}. \tag{7}$$

- The ν_1 stretching fundamental effective Hamiltonian (in polyad P_6),

$$\widetilde{H}^{<P_6(\nu_1)>} = H_{\{\mathrm{P}_0\}}^{<P_6(\nu_1)>} + H_{\{P_2\}}^{<P_6(\nu_1)>} + H_{\{P_3\}}^{<P_6(\nu_1)>} + H_{\{P_4\}}^{<P_6(\nu_1)>} + H_{\{P_5\}}^{<P_6(\nu_1)>} + H_{\{P_6(\nu_1)\}}^{<P_6(\nu_1)>}. \quad (8)$$

- The ν_3 stretching fundamental effective Hamiltonian (in polyad P_8),

$$\begin{aligned}\widetilde{H}^{<P_8(\nu_3)>} = & \\ & H_{\{\mathrm{P}_0\}}^{<P_8(\nu_3)>} + H_{\{P_2\}}^{<P_8(\nu_3)>} + H_{\{P_3\}}^{<P_8(\nu_3)>} + H_{\{P_4\}}^{<P_8(\nu_3)>} + H_{\{P_5\}}^{<P_8(\nu_3)>} + H_{\{P_6(\nu_1)\}}^{<P_8(\nu_3)>} \\ & + H_{\{P_7\}}^{<P_8(\nu_3)>} + H_{\{P_8(\nu_3)\}}^{<P_8(\nu_3)>}. \end{aligned} \quad (9)$$

For the last two cases, the ν_1 and ν_3 fundamental bands are part of larger polyads (P_6 and P_8, respectively), owing to the polyad scheme definition in Equation (1); however, the present effective Hamiltonien fit (see below) shows no clear perturbation of $v_1 = 1$ and $v_3 = 1$ from the other polyad levels. As a consequence, we use here restricted versions of polyads P_6 and P_8 by including only the fundamental levels. Intra-polyad interactions may be included in a future study, when transitions to the other levels in these polyads (which are likely to be weak transitions) will be assigned, which is not the case at present. Polyads P_4, P_5 and P_6 are included as defined in Equation (1) and on Figure 2 in the calculation and fit jobs, but their parameters are not used in the present fits so that their values can be kept fixed to zero.

3.3. Effective dipole moment operator

In order to calculate line intensities, we use the dipole moment effective operator, which is expanded in a similar way as for the effective Hamiltonian (see previous section). This development is explained in Refs. [31, 32, 36].

Since we do not consider here absolute intensities for the $\nu_4 - \nu_2$ and $\nu_1 - \nu_4$ transitions and only approximate intensities for ν_2-GS (and ν_1-GS, see below), the dipole moment operator was expanded at the minimum order for these three transitions, that is 1. The ν_2 fundamental band of E symmetry is forbidden in first approximation but gains intensity through the coupling with other bands (presumably mainly ν_4 in this case, as for many other tetrahedral molecules like CH_4 [37], CF_4 [38], GeH_4 [39, 40], RuO_4 [41], OsO_4 [42], *etc.*). In the present study, we do not analyze it in an interacting dyad, but rather as an isolated band since it appears to constitute the single vibrational level polyad P_2 in the scheme define above. As a consequence, interactions with other bands are small perturbations that can be considered as negligible for line position calculations; isolating the polyads by treating inter-polyad interactions through contact transformations would lead to a first order effective dipole moment operator:

$$\widetilde{\mu}^{\langle\nu_2-\mathrm{GS}\rangle} = \mu_{\nu_2}^1 \left(R^{1(1,0F_1)} \otimes {}^{-}V_{\{GS\}\{\nu_2\}}^{1(A_1E)E} \right)^{(F_2)}. \quad (10)$$

We provide below an estimate of the associated parameter $\mu_{\nu_2}^1$, see Section 4.5

As for the $\nu_4 - \nu_2$ difference band, we have an order 1 purely vibrational effective dipole moment operator:

$$\widetilde{\mu}^{\langle \nu_4 - \nu_2 \rangle} = \mu^1_{\nu_4 - \nu_2} {}^{+}V^{1(EF_2)F_2}_{\{\nu_2\}\{\nu_4\}}, \tag{11}$$

while for the $\nu_1 - \nu_4$ difference band, we have in the same way also at an order 1:

$$\widetilde{\mu}^{\langle \nu_1 - \nu_4 \rangle} = \mu^1_{\nu_1 - \nu_4} {}^{+}V^{1(F_2A_1)F_2}_{\{\nu_4\}\{\nu_1\}}. \tag{12}$$

For these two bands, this thus amounts to only one parameter ($\mu^1_{\nu_4-\nu_2}$ and $\mu^1_{\nu_1-\nu_4}$, respectively) whose value is simply set to 1 in order to calculate relative intensities.

We show below in Section 4.4 that the totally symmetric ν_1 stretching fundamental with A_1 symmetry is itself slightly observable. Again, this is a "forbidden band", but rovibrational couplings with other bands, as for GeH_4 [43] or OsO_4 [44], *etc.*, can give it some small intensity. Contact transformations would lead to an order 2 effective dipole moment operator:

$$\widetilde{\mu}^{\langle \nu_1 - \mathrm{GS} \rangle} = \mu^2_{\nu_1} \left(R^{2(2,0F_2)} \otimes {}^{+}V^{1(A_1A_1)A_1}_{\{GS\}\{\nu_1\}} \right)^{(F_2)}, \tag{13}$$

with one parameter, $\mu^2_{\nu_1}$.

In the case of the ν_3-GS and ν_4-GS transitions, their effective dipole moment operator is expanded exactly as described in Section 3.2 of our previous SiF_4 paper [15]. This allows to calculate absolute intensities of the ν_3 and ν_4 bands in order to update the TFSiCaSDa database, see Section 5 below.

3.4. Basis sets and line intensities

The calculation of the effective Hamiltonian and effective dipole moment matrix elements are performed in the coupled rovibrational basis

$$\left| \left[\Psi_v^{(C_v)} \otimes \Psi_r^{(J,nC_r)} \right]^{(C)}_{\sigma} \right\rangle, \tag{14}$$

where $\Psi_r^{(J,nC_r)}$ is a rotational wavefunction with angular momentum J, rotational symmetry species C_r and multiplicity index n; $\Psi_v^{(C_v)}$ is a coupled vibrational basis set with symmetry species C_v; C is the overall symmetry species ($C = C_v \otimes C_r$), with component σ. In the present case, $\Psi_v^{(C_v)}$ contains the relevant functions for the ν_1, ν_2, ν_3 or ν_4 normal modes of vibration ,

$$\left| \Psi^{(C_v)}_{v\ \sigma_v} \right\rangle = \left| \left(\left(\left(\Psi^{(C_1)}_{v_1} \otimes \Psi^{(l_2,C_2)}_{v_2} \right)^{(C_2)} \otimes \Psi^{(l_3,n_3C_3)}_{v_3} \right)^{(C_{23})} \otimes \Psi^{(l_4,n_4C_4)}_{v_4} \right)^{(C_v)}_{\sigma_v} \right\rangle, \tag{15}$$

with:

- For the non-degenerate mode ν_1, we use a symmetrized one-dimensional harmonic oscillator basis set denoted

$$\left| \psi^{(C_1)}_{v_1} \right\rangle = |v_1, C_1\rangle, \tag{16}$$

  with $v_1 = 1$ for the fundamental band, v_1 being the usual vibrational quantum numbers and $C_1 = A_1$.

- For the doubly degenerate mode ν_2, we use a symmetrized doubly degenerate harmonic oscillator basis set denoted

$$\left|\psi_{v_2\ \sigma_2}^{(l_2,C_2)}\right\rangle = |v_2, l_2, C_2, \sigma_2\rangle\,, \tag{17}$$

  with v_2 and l_2 being the usual vibrational and vibrational angular momentum quantum numbers, respectively; in the case of the fundamental band, $v_2 = l_2 = 1$ and $C_2 = E$, $\sigma_2 = 1$ or 2.

- For the triply degenerate modes ν_3 and ν_4, we use a symmetrized triply degenerate harmonic oscillator basis set denoted

$$\left|\psi_{v_i\ \sigma_i}^{(l_i,n_iC_i)}\right\rangle = |v_i, l_i, n_i, C_i, \sigma_i\rangle\,, \tag{18}$$

  with $i = 3$ or 4, v_i and l_i being the usual vibrational and vibrational angular momentum quantum numbers, respectively, while n_i is a multiplicity index; $v_i = l_i = 1$ and $C_i = F_2$, $\sigma_i = x$, y or z in the case of fundamental bands.

In Eq. (15), C_{23} is an intermediate symmetry species:

$$C_{23} = C_2 \otimes C_3. \tag{19}$$

The effective Hamiltonian matrix expressed in basis (14) is diagonalized numerically, and this leads to eigenfunctions obtained from

$$\widetilde{H}\left|\Psi_\sigma^{(J,C,\alpha)}\right\rangle = E\left|\Psi_\sigma^{(J,C,\alpha)}\right\rangle, \tag{20}$$

where $\alpha = 1, 2, \ldots$ numbers functions with the same symmetry C within a given J block. This eigenbasis set can be expanded in terms of the initial rovibrational basis set (14) and is used to calculate the matrix elements (in Debye) of the Z component μ_Z of the effective dipole moment operator $\widetilde{\mu}$, in the laboratory-fixed frame. This μ_Z component is related to $\widetilde{\mu}$ through Stone coefficients [45] and the direction cosines tensor as explained in Section 6.1. of Ref. [32].

The absolute line intensity (especially in the case of the ν_3 or ν_4 band for the TFSiCaSDa database [15], see Section 5 below) at temperature T for a transition at wavenumber $\widetilde{\nu}_{if}$ (in cm^{-1}) between an initial state i (with energy E_i, in Joules) and a final state f is then obtained through:

$$S_{if}(\mathrm{cm}^{-1}/(\mathrm{molecule.cm}^{-2})) = \frac{1}{4\pi\varepsilon_0}\widetilde{\nu}_{if}\frac{8\pi^3}{3hcQ}e^{-\frac{E_i}{k_BT}}\left(1 - e^{-\frac{hc\widetilde{\nu}_{if}}{k_BT}}\right)R_{if}, \tag{21}$$

with

$$R_{if} = 3\sum_{\alpha_i,\alpha_f}\left|\left\langle\Psi_{\sigma_f}^{(J_i,C_i,\alpha_i)}\right|\mu_Z\left|\Psi_{\sigma_f}^{(J_f,C_f,\alpha_f)}\right\rangle\right|^2. \tag{22}$$

Q is the total partition function at temperature T [46], c the speed of light in vacuum, h Planck's constant and k_B Boltzmann's constant. The line strength S_{if} is expressed here in the so-called "HITRAN unit" [47].

4. Analysis and discussion

4.1. Line positions

We have expanded the effective Hamiltonian up to order 6 for all polyads from P_0 to P_8 (but polyads P_4, P_5 and P_7 are not used is the present study, see Section 3.1).

Since the aim of the present work is to get accurate effective Hamiltonian parameters for the ground and all four fundamental vibrational states ($v_i = 1$ with $i = 1$ to 4), we chose to assign and fit together three of the far infrared bands that can be seen in Figure 1, that are ν_2-GS, $\nu_1 - \nu_4$ and $\nu_4 - \nu_2$, together with the ν_3-GS, ν_4-GS fundamental bands from our previous paper [15]; as in this one, we also included microwave rotational transitions from GS−GS and $\nu_3 - \nu_3$ taken from the paper of Jörissen *et al.* [14].

Some other bands (for instance $\nu_3 - \nu_1$, $\nu_2 - \nu_1$ or $\nu_3 - \nu_4$) shown in Figure 1 were not considered here, being either too weak or overlapping with nearby overtone or combination bands. These ones will be considered at a later stage, when performing an even more global study of full SiF_4 polyads up to the near-infrared region. Isotopologues $^{29}SiF_4$ and $^{30}SiF_4$ were not considered here either, the far-infrared region being somewhat noisy and their lines being too weak to be identified.

The well isolated ν_2 spectrum was quite easy to assign, starting with approximate low-order parameters set up by hand and then assigning and fitting more and more lines. Assignments were performed using the SPVIEW program [33] and spectrum fits, calculations and simulations were obtained through the XTDS program suite [33] dedicated to the modeling of highly-symmetrical molecules and implementing the tensorial formalism described above.

Since the $v_4 = 1$ level is well-known from Ref. [15], it was easy to perform an initial simulation of the $\nu_1 - \nu_4$ difference band; the structure of the totally symmetric $v_1 = 1$ level is very simple and one can just start by setting by hand its band center. The band was then straightforward to assign.

In the same way, once a first fit gave reliable parameters for $v_2 = 1$, it was easy to simulate and assign the $\nu_4 - \nu_2$ difference band. This is the lowest band we could observe in our spectra (125 cm^{-1} region).

We could thus perform a global fit of almost 20 000 lines pertaining to seven transitions of $^{28}SiF_4$: GS−GS ($P_0 - P_0$), ν_2-GS ($P_2 - P_0$), ν_4-GS ($P_3 - P_0$), $\nu_4 - \nu_2$ ($P_3 - P_2$), $\nu_1 - \nu_4$ ($P_6 - P_3$), ν_3-GS ($P_8 - P_0$) and $\nu_3 - \nu_3$ ($P_8 - P_8$). The resulting 59 effective Hamiltonian parameters are given in Table 2. Figure 3 details the fit residuals for line positions for these seven types of transitions, along with some statistics. We can see that we obtain a very satisfying result. In the case of the ν_2, ν_3 and ν_4 bands, some systematic deviations are observed at high rotational quantum number J values (similarly to what was already observed for ν_3 and ν_4 in Ref. [15]), but these stay very small ; this may indicate some small perturbations that will be treated at a later stage, when we perform a more global study.

4.2. Spectrum simulations and energy levels

In this section, we illustrate our results by showing some spectrum simulations, compared to the experiment, for the new bands recorded in the far-infrared region. The resulting

simulations for ν_3 and ν_4 are extremely similar to those obtained in our previous paper dedicated to these the strongly absorbing fundamentals [15].

Figure 4 shows the comparison of the experimental and simulated spectrum for ν_2, with a detail in its P branch being shown in Figure 5. The fine structure of the band is nicely reproduced.

Figure 6 shows the reduced rovibrational energy levels for the $v_2 = 1$ vibrational level of $^{28}SiF_4$, defined by

$$\begin{aligned} \widetilde{\nu}_{\rm red} &= \widetilde{\nu} - \sum_{\Omega} t^{\Omega(0,0A_1)A_1A_1}_{\{\rm GS\}\{\rm GS\}} (J(J+1))^{\Omega/2} \\ &= \widetilde{\nu} - B_0 J(J+1) + D_0 J^2(J+1)^2 - H_0 J^2(J+1)^4 + L_0 J^6(J+1)^6 \ldots, \end{aligned} \quad (23)$$

i.e. we subtract the dominant scalar polynomial terms in order to enhance levels splittings due to molecular symmetry. We give both the calculated and observed reduced energy levels. Observed levels are simply levels reached by assigned transitions which are included in the fit. This gives a good idea of the sampling of the energy spectrum. This one looks quite good here, up to high J values.

Figures 7 and 8 compare experiment and simulation for the $\nu_4 - \nu_2$ and $\nu_1 - \nu_4$ difference bands, respectively. Some inserts show again that the fine structure is very well modeled.

4.3. Equilibrium bond length

The determination of the equilibrium bond length r_e of a spherical-top molecule (which is the unique geometrical parameter that defines its equilibrium structure) is possible if one knows the value of the rotational constant B_0 in the ground state and rotational constant differences in all the vibrational fundamental levels, say $\Delta B_i = B_i - B_0$ ($i = 1$ to 4), where B_i is the rotational constant in an excited state with $v_i = 1$ [48]. The formula giving B_e (equilibrium value) is [42]:

$$B_e = B_0 - \frac{1}{2} \sum_{i=1}^{4} d_i \Delta B_i, \quad (24)$$

where d_i is the normal mode degeneracy ($d_1 = 1$, $d_2 = 2$, $d_3 = d_4 = 3$). The equilibrium bond length is then [42]:

$$r_e = \sqrt{\frac{3h}{64\pi^2 c m_{\rm F} B_e}}, \quad (25)$$

h being Planck's constant, c the speed of light in vacuum and $m_{\rm F}$ the fluorine atom mass, whose values are taken from Ref. [49]. The fitted parameters $B_0 = t^{2(0,0A_1)A_1A_1}_{\{0\}\{0\}}$ and $\Delta B_i = t^{2(0,0A_1)\Gamma_v\Gamma_v}_{\{i\}\{i\}}$ ($i = 1$ to 4) result from the line position fits in Table 2. Using these fitted values, we get:

$$B_e = 0.13819608(52)\ {\rm cm}^{-1}, \quad (26)$$

and thus:

$$r_e({\rm SiF_4}) = 1.5516985(30)\ {\rm \AA}. \quad (27)$$

Although this is determined from $^{28}SiF_4$ only, it should be recalled that, within the Born-Oppenheimer approximation, structural parameters like r_e do not depend on the isotopologue. It was not possible, using the present data, to assign lines in the ν_2 and $\nu_1 - \nu_4$ bands of the $^{29}SiF_4$ and $^{30}SiF_4$ isotopologues since they appeared too weak in our spectra (contrary to the case of the ν_3 and ν_4 very strong fundamental band for which lines of these low-abundance isotopologues were assigned in our previous work [15]). However, we could get a very high (1σ) accuracy, due to the very precise B_0 and ΔB_i values obtained in the present fit of 19 432 high-resolution infrared transitions (see Table 2).

Somewhat higher values can be found in rather old references, as mentioned in the Introduction. The *CRC Handbook of Chemistry and Physics* [50] reports an experimental value $r_e = 1.553$ Å of unknown origin, while Hagen and Hedberg [17] found $r_e = 1.552(2)$ Å using electron diffraction. Beagley *et al.* [16] report $r_e = 1.555(2)$ Å using the same technique. The most accurate study was up to now the theoretical one of Breidung *et al.*, using an *ab initio* calculation and giving $r_e = 1.5524(8)$ Å [18]. This last value is compatible with ours, although just at the limit of the uncertainty interval.

4.4. Direct observation of the ν_1 fundamental band

In the case of SiF_4, the ν_1 fundamental band itself appears to be very weak. As a "forbidden" band (in first approximation) it gets some intensity from coupling with other modes, as in the case of ν_2. But ν_1 is difficult to observe ; it is also very close to the strong $2\nu_4$ overtone and partially blended by it. We could, however, observe it in our mid-infrared spectrum that will be exploited in a future paper.

As shown in Figure 9, the accurate ν_1 parameters obtained in the work allowed us to simulate ν_1 (using a single order 2 effective dipole moment parameter, see Section 3.3 and below) and this compares well with the experiment. The region is, however very noisy and the ν_1 lines are too weak to be correctly exploited for the present purpose of an accurate determination of fundamental level parameters; these ones are well fitted thanks to the $\nu_1 - \nu_4$ difference band lines. It is however very satisfying that ν_1 is correctly predicted and observed.

4.5. Estimates of fundamental band intensities

It is interesting for future theoretical studies to estimate, even roughly, the order of magnitude of the band intensities for all fundamental bands. In the case of the A_1 and E symmetry fundamental regions (IR–forbidden in a first approximation but weakly activated by rotational resonances, see Section 3.3), we did not performed sufficient measurements to attempt a true, line-by-line intensity analysis, but can draw a rough estimate from the total integrated intensities at low temperatures.

So, the situation for all four fundamental bands summarizes as follows, in decreasing order of accuracy:

- In our previous study [15], we could make a rather accurate estimate of the ν_3 strong stretching fundamental integrated intensity of 691 km/mol, leading to a dipole moment derivative $\mu^0_{\nu_3} = 0.5444(38)$ D (see Table 3 of [15]).

- This same reference [15] did not include the case of the ν_4 bending fundamental intensity. But we can make here an estimate of 125(20) km/mol for this band from our previous measurements. This last value compares well with the value of 133 km/mol in Ref. [51]. It allows to estimate the dipole moment derivative to be $\mu^0_{\nu_4} \simeq 0.3706$ D. As this is just a quick estimate that does not use individual line strengths, we do not provide any uncertainty. The simulation for $^{28}SiF_4$ shows a good overall agreement as illustrated by Figure 10. This result has been used to update our TFSiCaSDa database [25], see Section 5.

- For the E-symmetry ν_2 band, we can derive a band intensity of about 0.8(1) km/mol. We can thus estimate the effective dipole moment parameter for the ν_2 band, as described by Eq. (10) in Section 3.3, to be roughly $\mu^1_{\nu_2} \simeq 6.2 \times 10^{-4}$ D.

- For the estimation of the very weak ν_1 band, which is severely overlapped by the IR-allowed $2\nu_4$ band (0.08 km/mol [15]), the situation is more difficult. We could just tune the dipole moment parameter (see Eq. (13) in Section 3.3) by hand and got a value of roughly $\mu^2_{\nu_1} \simeq 4.7 \times 10^{-7}$ D, leading to an estimate of the ν_1 integrated intensity of 0.02 km/mol. This should be more viewed as an order of magnitude than an accurate determination.

5. TFSiCaSDa database update

Dijon spectroscopic databases [25] contain calculated spectroscopic line lists for line positions, line intensities, full rovibrational transition labels and much more. These calculations are derived from experimental spectroscopic analyses where lines are assigned using the SPVIEW software [33] while Hamiltonians and dipole moments parameters are fitted with XTDS [33] software. By September 2021, 8 molecules are described in 8 databases. These databases are developed in the framework of the international consortium VAMDC (Virtual Atomic and Molecular Data Centre, `http://vamdc.org`) [52, 53, 54, 55] and are also part of the Dat@OSU project (`http://dataosu.obs-besancon.fr`).

The present work allowed us to extend our SiF_4 database (TFSiCaSDa) [25] with the addition of 147 333 new lines that belong to the ν_4 band, whose absolute intensity parameter has been estimated in this work (see Section 4.5). So far, and for the sake of simplicity, we do not use the polyad scheme as described in Section 3.1 to construct the database and both bands are treated separately. Table 3 presents the result of the database contents. The calculated lines have thus been introduced using two different schemes for the three isotopologues. Scheme 1 stands for ν_3 (*i.e.* P_1 is just the $v_3 = 1$ level) and scheme 2 for the newly included ν_4 band (*i.e.* P_1 is just the $v_4 = 1$ level). Our webpage (`http://vamdc.icb.cnrs.fr/PHP/SiF4.php`) allows to plot the data and download two sorts of file formats: the line by line list is given following the HITRAN 2004 format [56], while the cross section list is a simple 2-column flat file. An overview of the TFSiCaSDa database is displayed in Figure 11, as downloadable from our website.

6. Conclusion

In a continued effort to analyze and to provide reliable spectroscopic simulations of the infrared spectrum of SiF_4, we have recorded new far- and mid-infrared high-resolution spectra for this molecule. The new data were used to obtain accurate effective Hamiltonian parameters for all the fundamental bands of the $^{28}SiF_4$ isotopologue. These results allowed to perform an accurate determination of the Si-F bond length. We also provided several band intensity estimates and updated the VAMDC/TFSiCaSDa database.

It is noticeable that far-infrared high-resolution spectroscopy provides invaluable spectroscopic information for spherical-top molecules. Traditionally, the "forbidden" fundamental bands ν_1 and ν_2 of such species were studied with high-resolution stimulated spectroscopy, as in our previous works on CF_4 [57], GeD_4 [58], SF_6 [59, 48, 60] or OsO_4 [61]. This technique, however, is not very sensitive and has a quite limited resolution (around 3×10^{-3} cm^{-1}). In the case of the totally symmetric ν_1 fundamental band, only a Q branch can be observed, which limits the amount of lines that can be assigned. Far-infrared absorption spectroscopy can provide higher resolution and larger spectral coverage. In the case of the v_1 fundamental level, if this one can be accessed through a difference band whose other level is already known (like $v_3 = 1$ for the $\nu_3 - \nu_1$ band for SF_6 [23] or $v_4 = 1$ for the $\nu_1 - \nu_4$ band of SiF_4 in the present study), this gives access to P, Q and R lines, that is, to many more lines than in the Raman case.

Such results could stimulate future theoretical studies, by challenging *ab initio* calculations. From our side, we intend to continue the analysis of SiF_4 further, by including as many combination and overtone bands as possible, using the polyad scheme defined in Section 3.1. The aim is to perform a consistent global fit like in the case of CH_4 [62, 63], GeD_4 [64], CF_4 [38] or SiF_4 [65]. Such a global fit approach is especially adapted to a molecule with a well-defined polyad structure, which is the case of SiF_4 (see Section 3.1 and Figure 2). We also intend to try to study more bands of the $^{29}SiF_4$ and $^{30}SiF_4$ less-abundant isotopologues. When complete, this will allow to provide improved synthetic line lists in order to help remote-sensing *in situ* measurements for this species.

Acknowledgments

The authors wish to warmly thank Mr. Alex Jourdan and Mrs. Julie Muller from the Orano Group, France, for providing the SiF_4 sample that was used to record all the spectra presented in this work, as well as Synchrotron SOLEIL for supporting this work (Project 20200349).

References

[1] J. Wang, P. Bulkin, I. Florea, J.-L. Maurice, E. Johnson, Microcrystalline silicon thin films deposited by matrix-distributed electron cyclotron resonance plasma enhanced chemical vapor deposition using an SiF_4/H_2 chemistry, J. Phys. D: Appl. Phys. 49 (2016) 285203–1–285203–12.

[2] P. Francis, C. Chaffin, A. Maciejewski, C. Oppenheimer, Remote determination of SiF_4 in volcanic plumes: A new tool for volcano monitoring, Geophys. Res. Lett. 23 (1996) 249–242.

[3] T. Mori, M. Sato, Y. Shimoike, K. Notsu, High SiF_4/HF ratio detected in Satsuma-Iwojima volcano's plume by remote FT-IR observation, Earth Plan. Sp. 54 (2002) 249–256.
[4] E. Nicotra, M. Viccaro, C. Ferlito, R. Cristofolini, Influx of volatiles into shallow reservoirs at Mt. Etna volcano (Italy) responsible for halogen-rich magmas, Eur. J. Mineral. 22 (2010) 121–138.
[5] W. Stremme, I. Ortega, C. Siebe, M. Grutter, Gas composition of Popocatépelt volcano between 2007 and 2008: FTIR spectroscopic measurements of an explosive event during quiescent degassing, Earth Plan. Sc. Lett. 301 (2011) 502–510.
[6] N. Taquet, I. Meza Hernández, W. Stremme, A. Bezanilla, M. Grutter, R. Campion, M. Palm, T. Boulesteix, Continous measurements of SiF_4 and SO_2 by thermal emission spectroscopy: Insight from a 6-month survey at the Popocatépelt volcano, J. Volcanol. Geotherm. Res. 341 (2017) 255–268.
[7] N. Taquet, W. Stremme, M. Grutter, J. Baylón, A. Bezanilla, B. Schiavo, C. Rivera, R. Campion, T. Boulesteix, A. Nieto-Torres, R. Espinasa-Pereña, T. Blumenstock, F. Hase, Variability in the gas composition of the Popocatépelt volcano plume, Front. Earth Sci. 7 (2019) 114–1–114–14.
[8] W. Stremme, A. Krueger, R. Harig, M. Grutter, Volcanic SO_2 and SiF_4 visualization using 2-D thermal emission spectroscopy – Part 1: Slant-columns and their ratios, Atmos. Meas. Tech. 5 (2012) 275–288.
[9] A. Krueger, W. Stremme, R. Harig, M. Grutter, Volcanic SO_2 and SiF_4 visualization using 2-D thermal emission spectroscopy – Part 2: Wind propagation and emission rates, Atmos. Meas. Tech. 6 (2013) 47–61.
[10] P. G. Sennikov, A. V. Vodopyanov, S. V. Golubev, D. A. Mansfeld, M. N. Drozdov, Y. N. Drozdov, B. A. Andreev, L. V. Gavrilenko, D. A. Pryakhin, V. I. Shashkin, O. N. Godisov, A. I. Glasunov, A. J. Safonov, H.-J. Pohl, M. L. W. Thewalt, P. Becker, H. Riemann, N. V. Abrosimov, S. Valkiers, Towards 0.99999 ^{28}Si, Sol. State Comm. 152 (2012) 455–457.
[11] F. Königer, A. Müller, Molecular constants of SiF_4, GeF_4 and RuO_4. An improvement and the analysis of the IR-band contours of $\nu_3(F_2)$ low temperature measurements and by using isotopically pure compounds, J. Mol. Spectrosc. 65 (1977) 339–344.
[12] R. S. McDowell, M. J. Reisfeld, C. W. Patterson, B. J. Krohn, M. C. Vasquez, G. A. Laguna, Infrared spectrum and potential constants of silicon tetrafluoride, J. Chem. Phys. 77 (1982) 4337–4343.
[13] M. Takami, H. Kuze, Infrared-microwave double resonance spectroscopy of the SiF_4 ν_3 fundamental using a tunable diode laser, J. Chem. Phys. 78 (1983) 2204–2209.
[14] L. Jörissen, H. Prinz, W. A. Kreiner, C. Wenger, G. Pierre, G. Magerl, W. Schupita, The ν_3 fundamental of silicon tetrafluoride. Spectroscopy with laser sidebands, Can. J. Phys. 67 (1989) 532–542.
[15] V. Boudon, L. Manceron, C. Richard, High-resolution spectroscopy analysis of the ν_3, ν_4 and $2\nu_4$ bands of SiF_4 in natural isotopic abundance, J. Quant. Spectrosc. Radiat. Transfer 253 (2020) 107114–1–106114–20.
[16] B. Beagley, D. P. Brown, J. M. Freeman, The Si-F bond length in SiF_4 – A new electron diffraction study, J. Mol. Struct. 18 (1973) 337–338.
[17] K. Hagen, K. Hedberg, Interatomic distances and rms amplitudes of vibration of gaseous SiF_4 from electron diffraction, J. Chem. Phys. 59 (1973) 1549–1550.
[18] J. Breidung, J. Demaison, L. Margulès, W. Thiel, Equilibrium structure of SiF_4, Chem. Phys. Lett. 313 (1999) 713–717.
[19] P. Roy, J.-B. Brubach, M. Rouzières, O. Pirali, F. Kwabia Tchana, L. Manceron, AILES: La ligne infrarouge et THz sur rayonnement synchrotron SOLEIL, Revue de l'électricité et de l'électronique 2008 (3) (2008) 23–30.
[20] J.-B. Brubach, L. Manceron, M. Rouzières, O. Pirali, D. Balcon, F. Tchana, V. Boudon, M. Tudorie, T. Huet, A. Cuisset, P. Roy, Performance of the AILES THz-infrared beamline on SOLEIL for high resolution spectroscopy, AIP Conference Proceeding 1214 (2010) 81–84.
[21] F. Kwabia Tchana, F. Willaert, X. Landsheere, J.-M. Flaud, L. Lago, M. Chapuis, C. Herbeaux, P. Roy, L. Manceron, A new, low temperature long-pass cell for mid-infrared to terahertz spectroscopy and synchrotron radiation use, Review of Scientific Instruments 84 (9) (2013) 093101.
[22] V. Boudon, L. Manceron, F. Kwabia Tchana, M. Loëte, L. Lago, P. Roy, Resolving the forbidden band of SF_6, Phys. Chem. Chem. Phys. 16 (2014) 1415–1423.

[23] M. Faye, A. L. Ven, V. Boudon, L. Manceron, P. Asselin, P. Soulard, F. Kwabia Tchana, P. Roy, High-resolution spectroscopy of difference and combination bands of SF_6 to elucidate the $\nu_3 + \nu_1 - \nu_1$ and $\nu_3 + \nu_2 - \nu_2$ hot band structures in the ν_3 region, Mol. Phys. 112 (2014) 2504–2514.
[24] M. Faye, V. Boudon, M. Loëte, P. Roy, L. Manceron, Observation and analysis of the SF_6 $\nu_2 + \nu_4 - \nu_5$ band: Improved parameters for the $\nu_5 = 1$ state, J. Mol. Spectrosc. 325 (2016) 35–41.
[25] C. Richard, V. Boudon, M. Rotger, Calculated spectroscopic databases for the VAMDC portal: New molecules and improvements, J. Quant. Spectrosc. Radiat. Transfer 251 (2020) 107096.
[26] M. Faye, M. Bordessoule, B. Kanouté, J.-B. Brubach, P. Roy, L. Manceron, Improved mid infrared detector for high spectral or spatial resolution and synchrotron radiation use, Rev. Sci. Inst. 87 (2016) 063119.
[27] L. S. Rothman, D. Jacquemart, A. Barbe, D. C. Benner, M. Birk, L. R. Brown, M. R. Carleer, C. C. Jr., K. Chance, L. H. Coudert, V. Dana, V. M. Devi, J.-M. Flaud, R. R. Gamache, A. Goldman, J.-M. Hartmann, K. W. Jucks, A. G. Maki, J.-Y. Mandin, S. T. Massie, J. Orphal, A. Perrin, C. P. Rinsland, M. A. H. Smith, J. Tennyson, R. N. Tolechov, R. A. Toth, J. Vander Auwera, P. Varanasi, G. Wagner, The HITRAN 2004 molecular spectroscopic database, J. Quant. Spectrosc. Radiat. Transfer 96 (2005) 139–204.
[28] V. Boudon, M. Rey, M. Loëte, The vibrational levels of methane obtained from analyses of high-resolution spectra, J. Quant. Spectrosc. Radiat. Transfer 98 (2006) 394–404.
[29] S. Albert, S. Bauerecker, V. Boudon, L. R. Brown, J.-P. Champion, M. Loëte, A. Nikitin, M. Quack, Global analysis of the high resolution infrared spectrum of methane $^{12}CH_4$ in the region from 0 to 4800 cm^{-1}, Chem. Phys. 356 (2009) 131–146.
[30] B. Amyay, V. Boudon, Vibration-rotation energy levels and corresponding eigenfunctions of $^{12}CH_4$ up to the tetradecad, J. Quant. Spectrosc. Radiat. Transfer 219 (2018) 85–104.
[31] J.-P. Champion, M. Loëte, G. Pierre, Spherical top spectra, in: K. N. Rao, A. Weber (Eds.), Spectroscopy of the Earth's atmosphere and interstellar medium, Academic Press, San Diego, 1992, pp. 339–422.
[32] V. Boudon, J.-P. Champion, T. Gabard, M. Loëte, M. Rotger, C. Wenger, Spherical top theory and molecular spectra, in: M. Quack, F. Merkt (Eds.), Handbook of High Resolution Spectroscopy, Vol. 3, John Wiley & Sons, Ltd, Chichester, 2011, Ch. 39, pp. 1437–1460.
[33] C. Wenger, V. Boudon, M. Rotger, J. P. Sanzharov, J. P. Champion, XTDS and SPVIEW: Graphical tools for the analysis and simulation of high-resolution molecular spectra, J. Mol. Spectrosc. 251 (2008) 102–113.
[34] J. H. V. Vleck, On σ-type doubling and electron spin in the spectra of diatomic molecules, Phys. Rev. 33 (1929) 467–506.
[35] D. Sadovskii, B. Zhilinskii, Contact transformations in tensor formalism. Effective Hamiltonian and dipole moment for the ν_2, ν_4 dyad of tetrahedral molecules, J. Quant. Spectrosc. Radiat. Transfer 42 (6) (1989) 575–583.
[36] V. Boudon, J.-P. Champion, T. Gabard, M. Loëte, M. Rotger, C. Wenger, Spherical top theory and molecular spectra, in: M. Quack, F. Merkt (Eds.), Handbook of High-Resolution Spectroscopy, Vol. 3, Wiley, Chichester, West Sussex, United Kingdom, 2011, pp. 1437–1460.
[37] J.-P. Champion, J.-C. Hilico, C. Wenger, L. Brown, Analysis of the ν_2/ν_4 dyad of $^{12}CH_4$ and $^{13}CH_4$, J. Mol. Spectrosc. 133 (1989) 256–272.
[38] M. Carlos, O. Gruson, C. Richard, V. Boudon, M. Rotger, X. Thomas, C. Maul, C. Sydow, A. Domanskaya, R. Georges, P. Souard, O. Pirali, M. Goubet, P. Asselin, T. R. Huet, High-resolution spectroscopy and global analysis of CF_4 rovibrational bands to model its atmospheric absorption, J. Quant. Spectrosc. Radiat. Transfer 201 (2017) 75–93.
[39] O. N. Ulenikov, O. V. Gromova, E. S. Bekhtereva, N. I. Raspopova, A. V. Kuznetsov, C. Sydow, S. Bauerecker, High resolution analysis of GeH_4 in the dyad region: Ro-vibration energy structure of $^{70}GeH_4$ and line strengths of $^{M}GeH_4$ ($M = 70, 72, 73, 74, 76$), J. Quant. Spectrosc. Radiat. Transfer 236 (2019) 106581.
[40] C. Richard, V. Boudon, A. Rizopoulos, J. Vander Auwera, F. K. Tchana, Line positions and intensities

for the ν_2/ν_4 bands of 5 isotopologues of germane near 11.5 μm, J. Quant. Spectrosc. Radiat. Transfer 260 (2021) 107474–1–107474–11.

[41] S. Reymond-Laruinaz, M. Faye, V. Boudon, D. Doizi, L. Manceron, High-resolution infrared spectroscopy and analysis of the ν_2/ν_4 bending dyad of ruthenium tetroxide, J. Mol. Spectrosc. 336 (2017) 29–35.

[42] M. Louviot, V. Boudon, L. Manceron, P. Roy, D. Bermejo, R. Z. Martínez, High-resolution spectroscopy and structure of osmium tetroxide. A benchmark study on $^{192}OsO_4$, Inorg. Chem. 51 (2012) 10356–10365.

[43] V. Boudon, T. Grigoryan, F. Philipot, C. Richard, F. Kwabia Tchana, L. Manceron, A. Rizopoulos, J. Vander Auwera, T. Encrenaz, Line positions and intensities for the ν_3 band of 5 isotopologues of germane for planetary applications, J. Quant. Spectrosc. Radiat. Transfer 205 (2018) 174–183.

[44] M. Louviot, V. Boudon, L. Manceron, P. Roy, D. Balcon, High-resolution spectroscopy and analysis of the ν_1/ν_3 stretching dyad of osmium tetroxide, J. Quant. Spectrosc. Radiat. Transfer 113 (2012) 119–127.

[45] A. J. Stone, Transformation between Cartesian and spherical tensors, Mol. Phys. 29 (1975) 1461–1471.

[46] R. McDowell, Rotational partition function for spherical-top molecules, J. Quant. Spectrosc. Radiat. Transfer 38 (1987) 337–346.

[47] I. E. Gordon, L. S. Rothman, C. Hill, R. V. Kochanova, Y. Tan, P. F. Bernath, M. Birk, V. Boudon, A. Campargue, K. V. Chance, B. J. Drouin, J.-M. Flaud, R. R. Gamache, J. T. Hodges, D. Jacquemart, V. I. Perevalov, A. Perrin, K. P. Shine, M.-A. H. Smith, J. Tennyson, G. C. Toon, H. Tran, V. G. Tyuterev, A. Barbe, A. Csaszar, M. V. Devi, T. Furtenbacher, J. J. Harrison, A. Jolly, T. Johnson, T. Karman, I. Kleiner, A. A. Kyuberis, J. Loos, O. M. Lyulin, S. T. Massie, S. N. Mikhailenko, N. Moazzen-Ahmadi, H. S. P. Müller, O. V. Naumenko, A. V. Nikitin, O. L. Polyansky, M. Rey, M. Rotger, S. Sharpe, K. Sung, E. Starikova, S. A. Tashkun, J. V. Auwera, G. Wagner, J. Wilzewski, P. Wcisło, S. Yu, E. J. Zak, The HITRAN2016 Molecular Spectroscopic Database, J. Quant. Spectrosc. Radiat. Transfer 203 (2017) 3–69.

[48] V. Boudon, J. L. Doménech, D. Bermejo, H. Willner, High-resolution Raman spectroscopy of the ν_1 region and Raman-Raman double resonance spectroscopy of the $2\nu_1 - \nu_1$ band of $^{32}SF_6$ and $^{34}SF_6$. Determination of the equilibrium bond length of sulfur hexafluoride, J. Mol. Spectrosc. 228 (2004) 392–400.

[49] E. R. Cohen, T. Cvitas, J. G. Frey, B. Holmström, K. Kuchitsi, R. Marquardt, I. Mills, F. Pavese, M. Quack, J. Stohner, H. L. Strauss, M. Takami, A. Thor, Quantities, Units and Symbols in physical chemistry, Third edition, IUPAC and Royal Society of Chemistry, RSC, Cambridge, 2007.

[50] J. R. R. Jr., T. J. Bruno, M. J. Doa (Eds.), CRC handbook of chemistry and physics, CRC Press, 2020.

[51] A. P. Burtsev, V. N. Bocharov, S. K. Ignatov, T. D. Kolomiĭtsova, P. G. Sennikov, K. G. Tokhadze, L. A. Chuprov, D. N. Shchepkin, O. Schrems, Integral intensities of absorption bands of silicon tetrafluoride in the gas phase and cryogenic solutions: Experiment and Calculation, Optics Spectrosc. 98 (2005) 227–234.

[52] M. L. Dubernet, V. Boudon, J. L. Culhane, M. S. Dimitrijevic, A. Z. Fazliez, C. Joblin, F. Kupka, G. Leto, P. L. Sidaner, P. A. Loboda, H. E. Mason, N. J. Mason, C. Mendoza, G. Mulas, T. J. Millar, L. A. Nuñez, V. I. Perevalov, N. Piskunov, Y. Ralchenko, G. Rixon, L. S. Rothman, E. Roueff, T. A. Ryabchikova, A. Ryabtsev, S. Sahal-Bréchot, B. Schmitt, S. Schlemmer, J. Tennyson, V. G. Tyuterev, N. A. Walton, V. Wakelam, C. J. Zeippen, Virtual Atomic and Molecular Data Centre, J. Quant. Spectrosc. Radiat. Transfer 111 (2010) 2151–2159.

[53] M. L. Dubernet, B. K. Antony, Y. A. Ba, Y. L. Babikov, K. Bartschat, V. Boudon, B. J. Braams, H.-K. Chung, F. Daniel, F. Delahaye, G. D. Zanna, J. de Urquijo, A. Domaracka, M. Doronin, B. J. Drouin, M. S. Dimitrijevic, C. P. Endres, E. Quintas-Sanchez, A. Z. Fazliev, S. V. Gagarin, I. E. Gordon, U. Heiter, C. Hill, D. Jevremovic, C. Joblin, A. Kasprzak, E. Krishnakumar, G. Leto, P. A. Loboda, T. Louge, S. Maclot, B. P. Marinkovic, A. Markwick, T. Marquart, H. E. Mason, N. J. Mason, C. Mendoza, A. A. Mihajlov, T. J. Millar, N. Moreau, G. Mulas, G. Leto, Y. Pakhomov, P. Palmeri, S. Pancheshnyi, V. I. Perevalov, N. Piskunov, J. Postler, P. Gratier, P. Quinet, G. Rixon,

Y. Ralchenko, Y.-J. Rhee, L. S. Rothman, E. Roueff, T. Ryabchikova, S. Sahal-Bréchot, P. Scheier, S. Schlemmer, B. Schmitt, E. Stempels, J. Tennyson, V. G. Tyuterev, V. Vujcic, V. Wakelam, N. A. Walton, O. Zatsarinny, C. J. Zeippen, C. M. Zwolf, the VAMDC Consortium, The Virtual Atomic and Molecular Data Centre (VAMDC) consortium for astrophysics, Journal of Physics B 49 (2016) 074003–1–074003–18.

[54] N. Moreau, C. M. Zwolf, Y. A. Ba, C. Richard, V. Boudon, M.-L. Dubernet, The VAMDC portal as a major enabler of atomic and molecular data citation, Galaxies 6 (2018) 105.

[55] D. Albert, B. K. Antony, Y. A. Ba, Y. L. Babikov, P. Bollard, V. Boudon, F. Delahaye, G. Del Zanna, M. S. Dimitrijević, B. J. Drouin, M.-L. Dubernet, F. Duensing, M. Emoto, C. P. Endres, A. Z. Fazliev, J.-M. Glorian, I. E. Gordon, P. Gratier, C. Hill, D. Jevremović, C. Joblin, D.-H. Kwon, R. V. Kochanov, E. Krishnakumar, G. Leto, P. A. Loboda, A. A. Lukashevskaya, O. M. Lyulin, B. P. Marinković, A. Markwick, T. Marquart, N. J. Mason, C. Mendoza, T. J. Millar, N. Moreau, S. V. Morozov, T. Möller, H. S. P. Müller, G. Mulas, I. Murakami, Y. Pakhomov, P. Palmeri, J. Penguen, V. I. Perevalov, N. Piskunov, J. Postler, A. I. Privezentsev, P. Quinet, Y. Ralchenko, Y.-J. Rhee, C. Richard, G. Rixon, L. S. Rothman, E. Roueff, T. Ryabchikova, S. Sahal-Bréchot, P. Scheier, P. Schilke, S. Schlemmer, K. W. Smith, B. Schmitt, I. Y. Skobelev, V. A. Srecković, E. Stempels, S. A. Tashkun, J. Tennyson, V. G. Tyuterev, C. Vastel, V. Vujčić, V. Wakelam, N. A. Walton, C. Zeippen, C. M. Zwölf, A decade with VAMDC: Results and ambitions, Atoms 8 (2020) 76.

[56] L. Rothman, D. Jacquemart, A. Barbe, D. Chris Benner, M. Birk, L. Brown, M. Carleer, C. Chackerian, Jr., K. Chance, L. Coudert, V. Dana, V. Devi, J.-M. Flaud, R. Gamache, A. Goldman, J.-M. Hartmann, K. Jucks, A. Maki, J.-Y. Mandin, S. Massie, J. Orphal, A. Perrin, C. Rinsland, M. Smith, J. Tennyson, R. Tolchenov, R. Toth, J. Vander Auwera, P. Varanasi, G. Wagner, The hitran 2004 molecular spectroscopic database, J. Quant. Spectrosc. Radiat. Transfer 96 (2) (2005) 139–204.

[57] V. Boudon, D. Bermejo, R. Z. Martínez, High-resolution stimulated Raman spectroscopy and analysis of the ν_1, $2\nu_1 - \nu_1$, ν_2, $2\nu_2$, and $3\nu_2 - \nu_2$ bands of CF_4, J. Raman. Spectrosc. 44 (2013) 731–738.

[58] G. Pierre, V. Boudon, E. B. Mkadmi, H. Bürger, D. Bermejo, R. Martínez, Study of the fundamental bands of $^{70}GeD_4$ by high-resolution Raman and infrared spectroscopy: First experimental determination of the equilibrium bond length of germane, J. Mol. Spectrosc. 216 (2002) 408–418.

[59] D. Bermejo, R. Z. Martínez, E. Loubignac, V. Boudon, G. Pierre, Simultaneous analysis of the ν_2 Raman and $\nu_2 + \nu_6$ infrared spectra of the SF_6 molecule, J. Mol. Spectrosc. 201 (2000) 164–171.

[60] V. Boudon, J. L. Doménech, A. Ramos, D. Bermejo, H. Willner, High-resolution stimulated Raman spectroscopy and analysis of the ν_2, ν_5 and $2\nu_6$ bands of $^{34}SF_6$, Mol. Phys. 104 (16–17) (2006) 2653–2661.

[61] M. Louviot, V. Boudon, D. Bermejo, R. Z. Martínez, L. Manceron, High-resolution stimulated Raman spectroscopy and analysis of the ν_1 band of osmium tetroxide, J. Raman Spectrosc. 44 (2012) 63–69.

[62] B. Amyay, M. Louviot, O. Pirali, R. Georges, J. Vander Auwera, V. Boudon, Global analysis of the high temperature infrared emission spectrum of $^{12}CH_4$ in the dyad (ν_2/ν_4) region, The Journal of Chemical Physics 144 (2016) 024312–1–024312–15.

[63] B. Amyay, A. Gardez, R. Georges, L. Biennier, J. Vander Auwera, C. Richard, V. Boudon, New investigation of the ν_3 C–H stretching region of $^{12}CH_4$ through the analysis of high temperature infrared emission spectra, J. Chem. Phys. 148 (2018) 134306.

[64] V. Boudon, D. Radhouani, M. Loëte, R. Z. Martínez, D. Bermejo, High-resolution stimulated Raman spectroscopy and analysis of the ν_3 stretching band of GeD_4, J. Raman Spectrosc. 38 (2007) 559–562.

[65] M. Faye, V. Boudon, M. Loëte, P. Roy, L. Manceron, The high overtone and combination levels of SF_6 revisited at doppler-limited resolution: A global effective rovibrational model for highly excited vibrational states, J. Quant. Spectrosc. Radiat. Transfer 190 (2017) 38–47.

[66] J. Herranz, The rotational structure of the fundamental infrared bands of methane-type molecules, J. Mol. Spectrosc. 6 (1961) 343–359.

[67] A. Robiette, D. Gray, F. Birss, The effective vibration-rotation Hamiltonian for triply-degenerate fundamentals of tetrahedral XY_4 molecules, Mol. Phys. 32 (1976) 1591–1607.

Figures

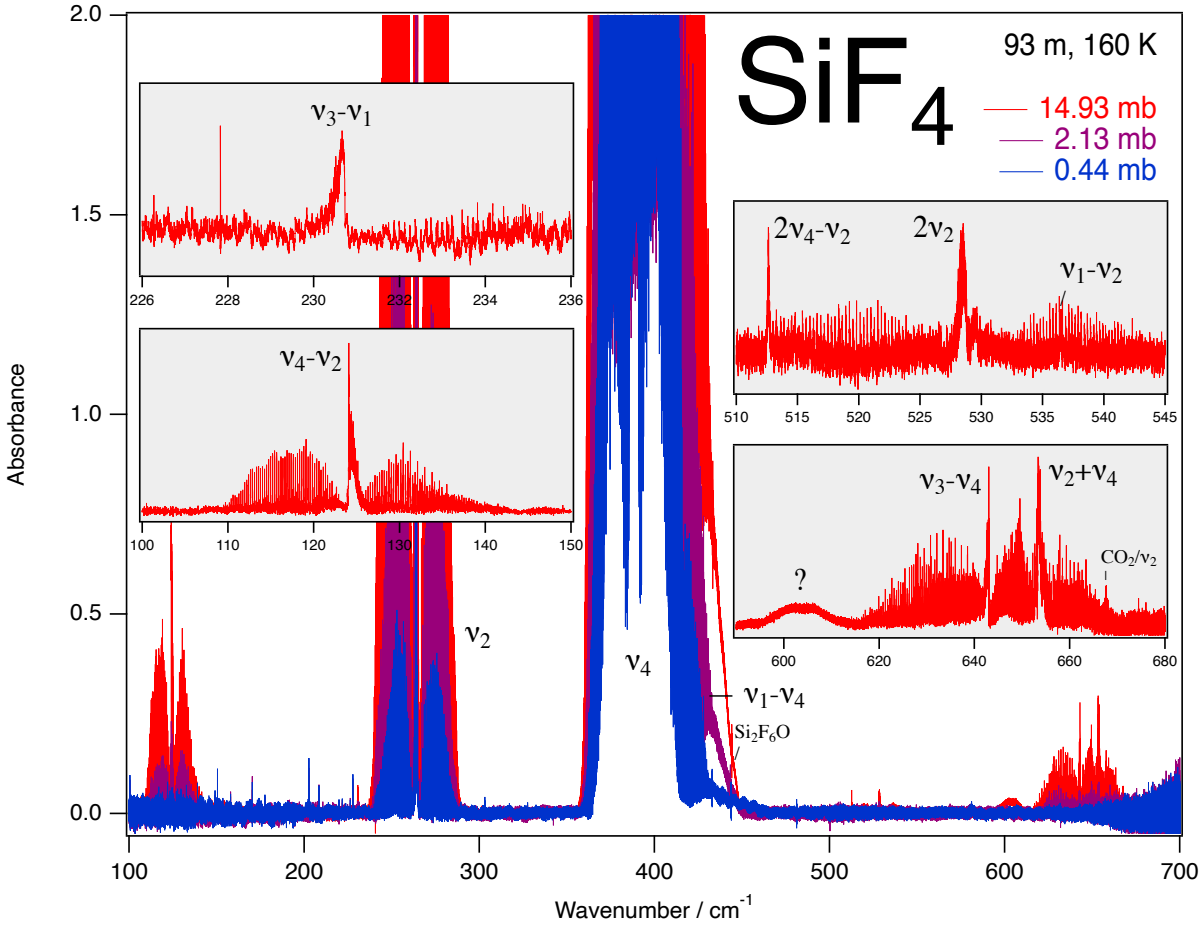

Figure 1: Overview of the far-infrared spectra of SiF_4 used in this paper. We can notice the presence of some impurities (CO_2, Si_2F_6O and another unknown one, marked by "?"). Here, we focus on ν_2, $\nu_4 - \nu_2$ and $\nu_1 - \nu_4$ (on the upper edge of ν_4); the other combination and overtone bands will be treated in a future paper.

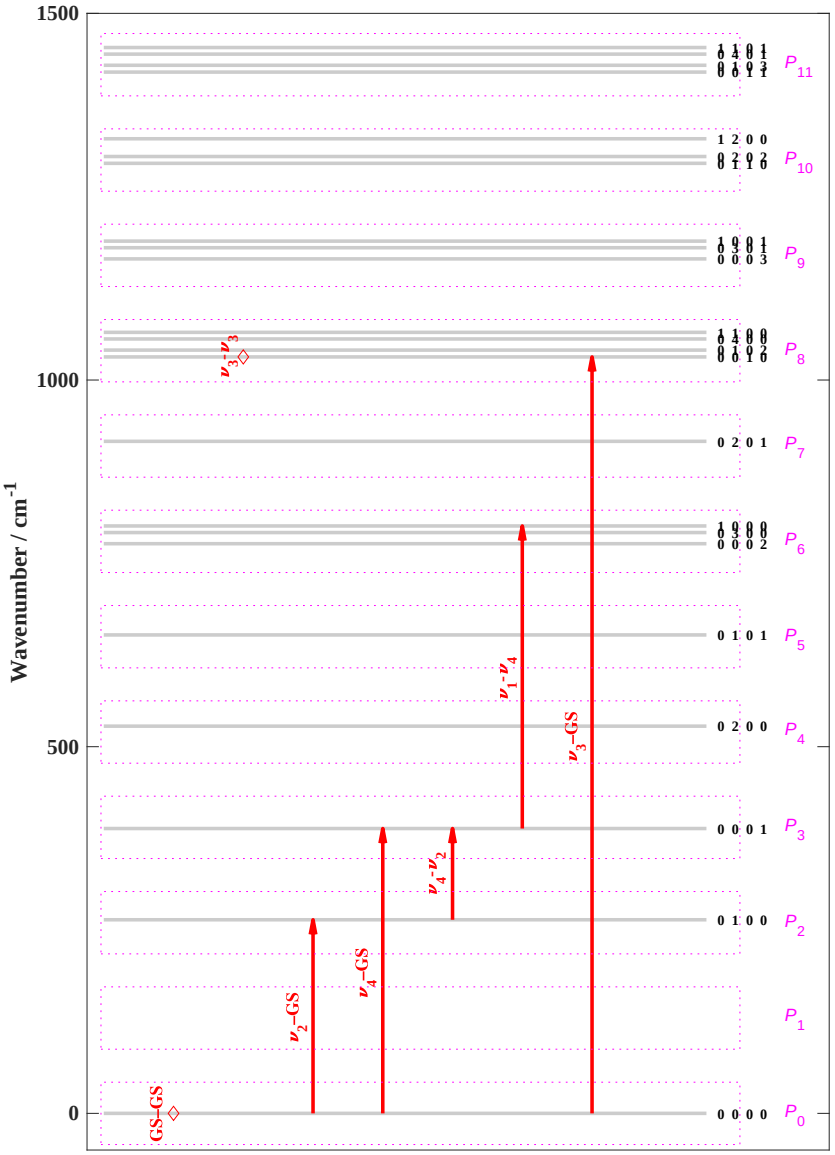

Figure 2: The vibrational polyads of $^{28}SiF_4$. Dashed pink rectangles delimit the polyads. Red arrows display the transitions used in the present study.

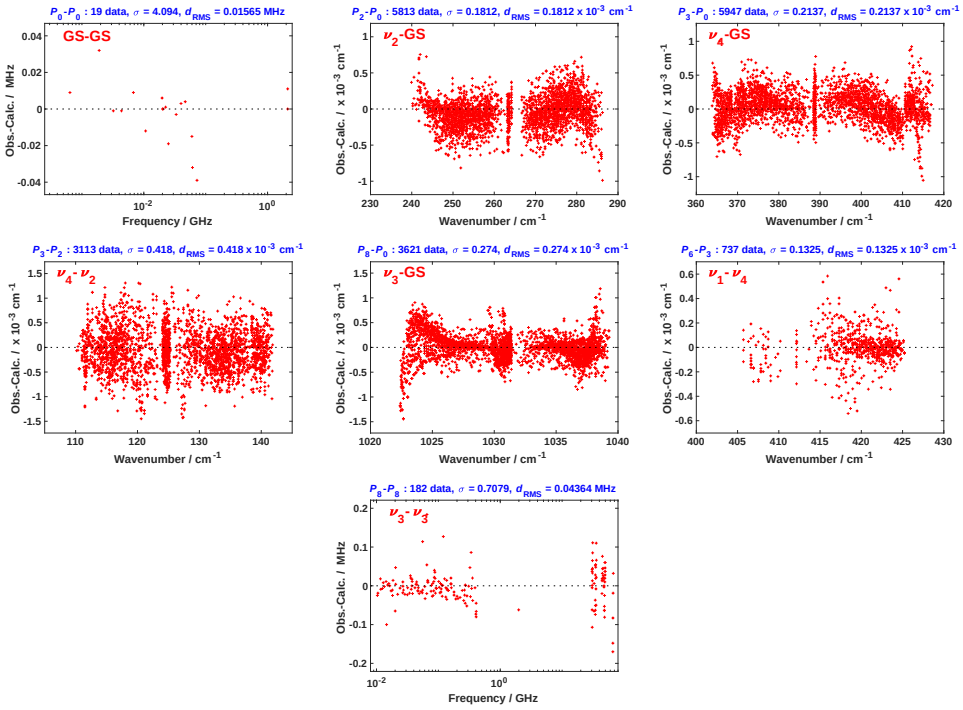

Figure 3: Fit residuals for line positions for the 7 different types of rovibrational transitions used in the present work.

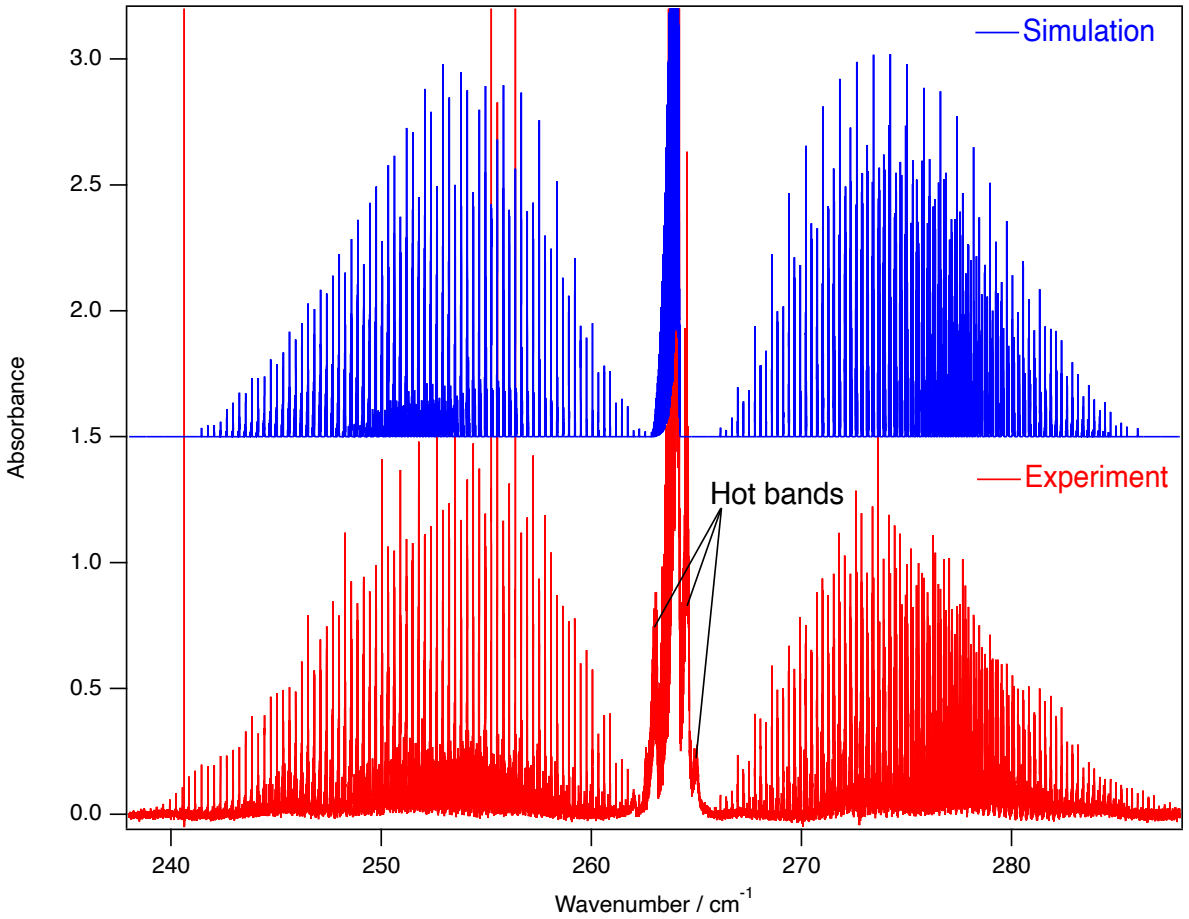

Figure 4: Overview of the ν_2 fundamental band, compared to the simulation. At least 3 Q branches from hot bands (not considered here) are visible.

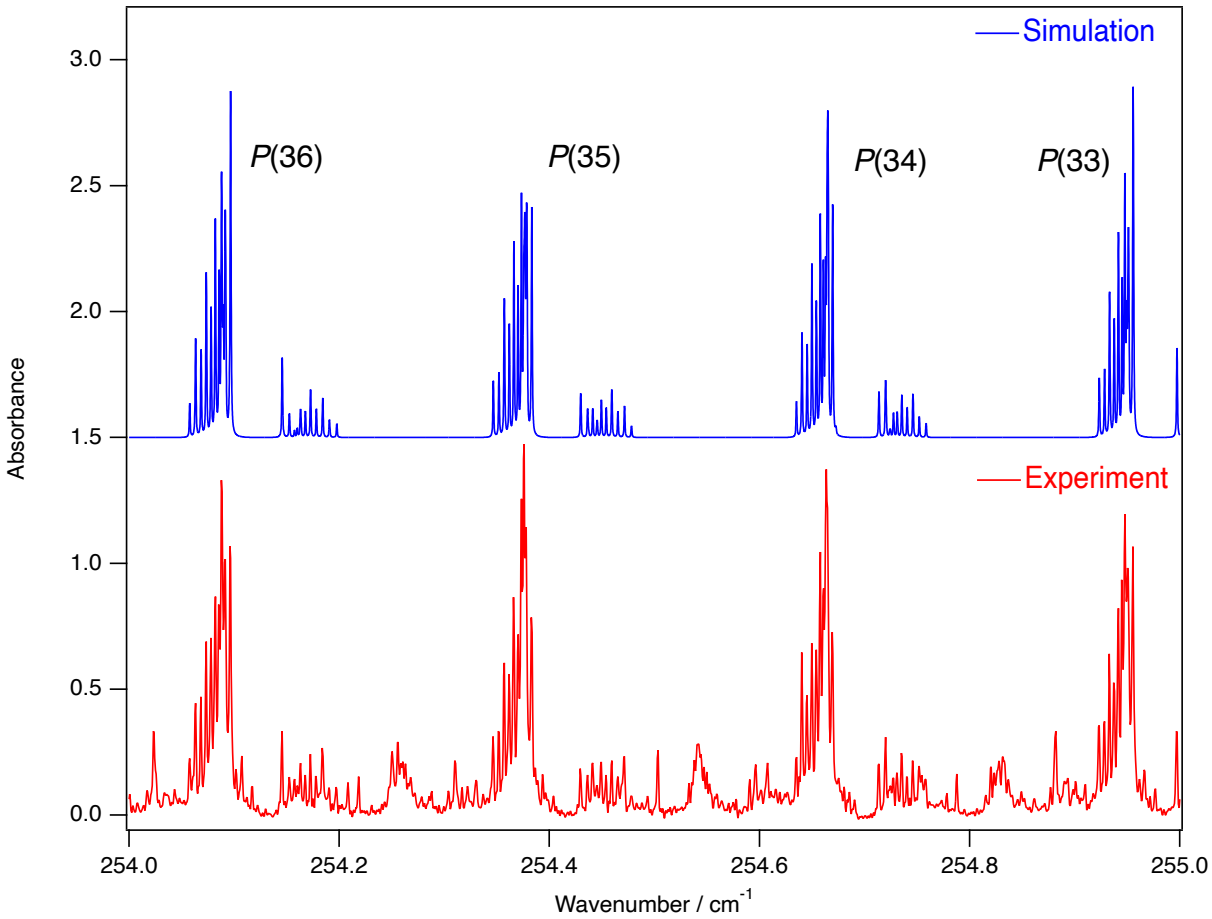

Figure 5: Detail in the P branch of the ν_2 fundamental band, compared to the simulation. Lines not present in the simulation are hot band lines, not considered here.

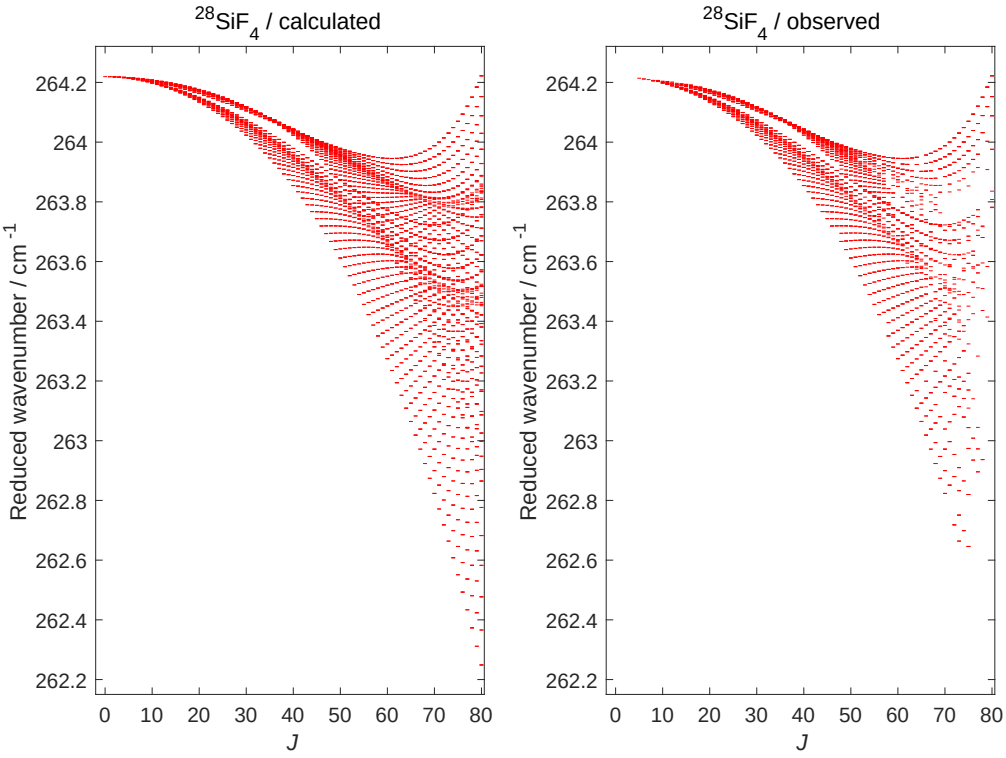

Figure 6: Calculated and observed rovibrational energy levels for the $v_2 = 1$ fundamental level. Observed levels are those reached by assigned transitions.

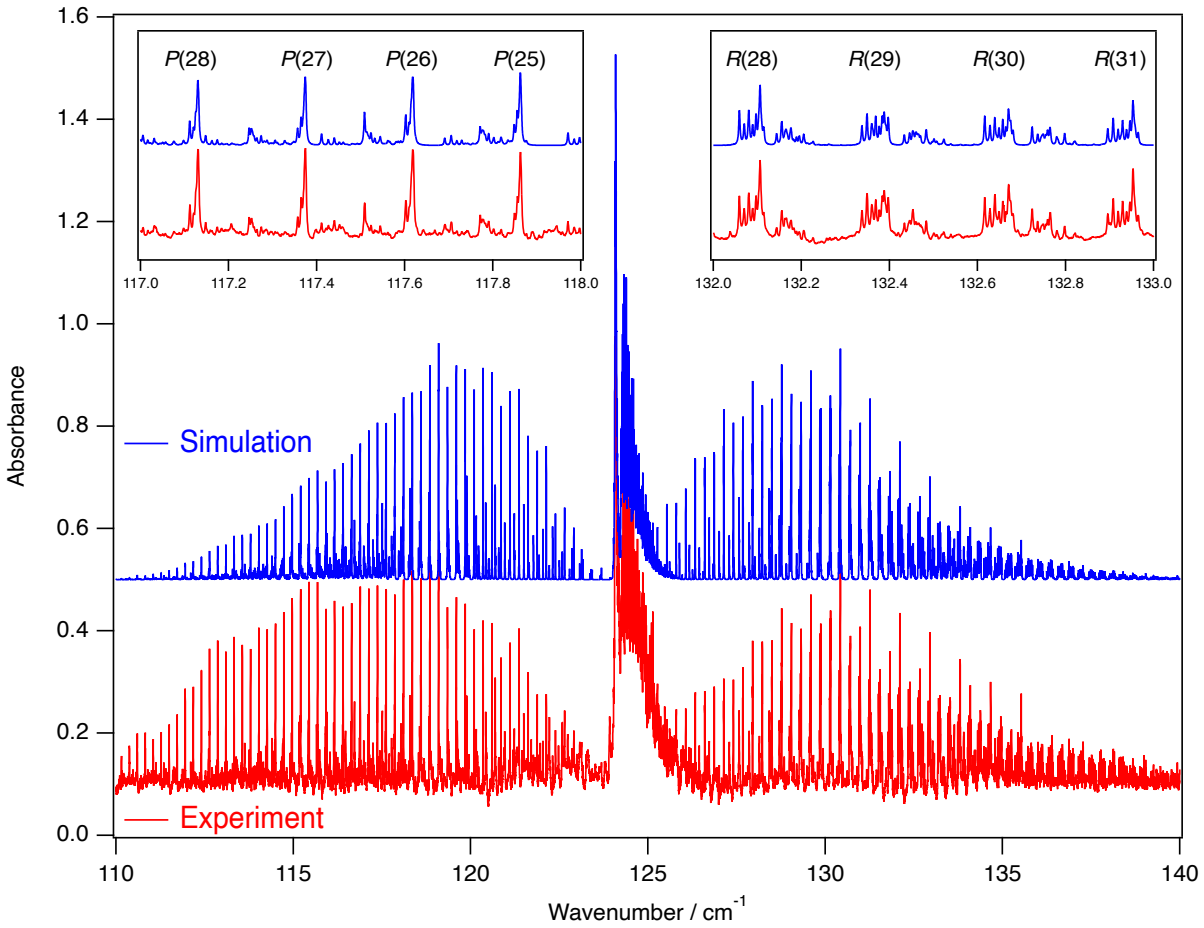

Figure 7: The $\nu_4 - \nu_2$ difference band, compared to the simulation. The inserts display a few line clusters in the P and R branches.

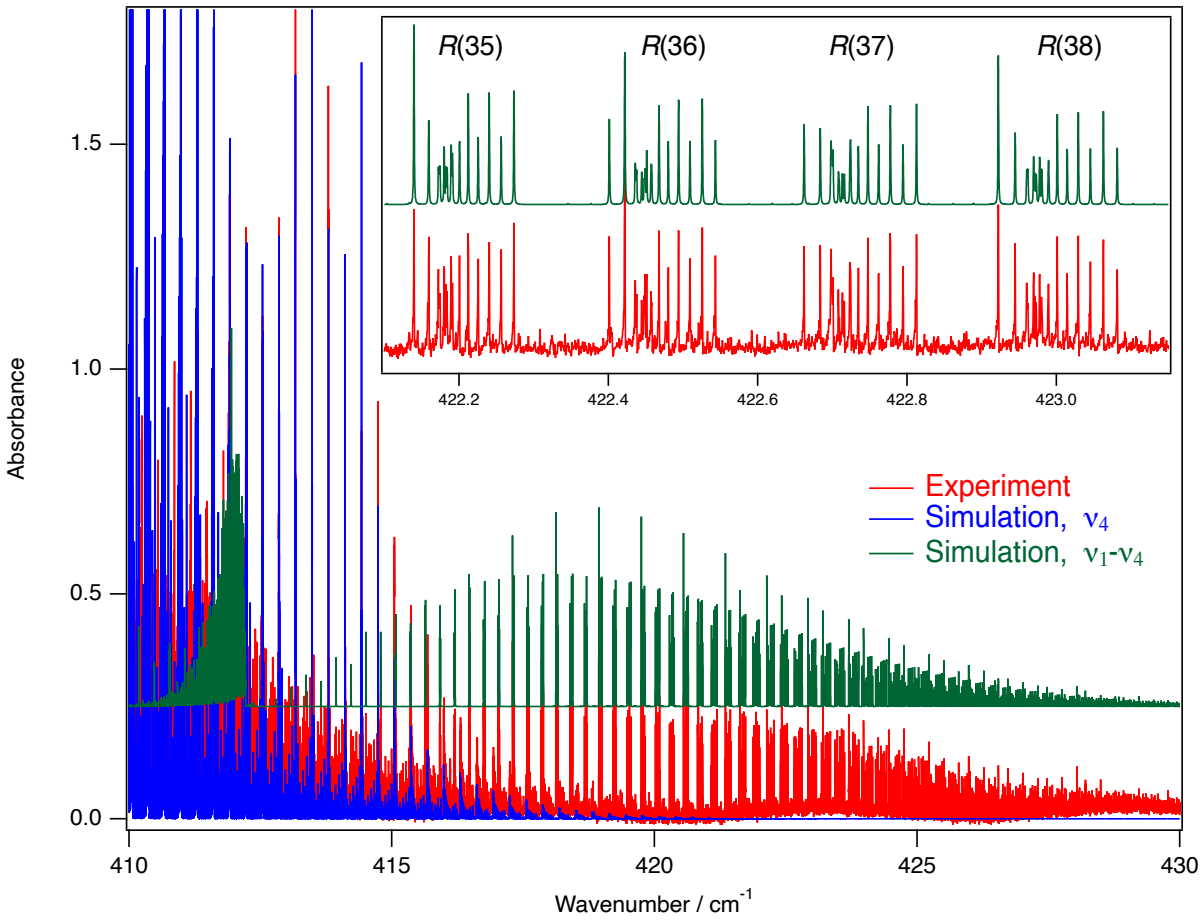

Figure 8: The R branch of the $\nu_1 - \nu_4$ difference band, compared to the simulation including also high-J lines of the ν_4 fundamental band. The insert displays a few line clusters, from $J = 35$ to 38, showing the excellent agreement.

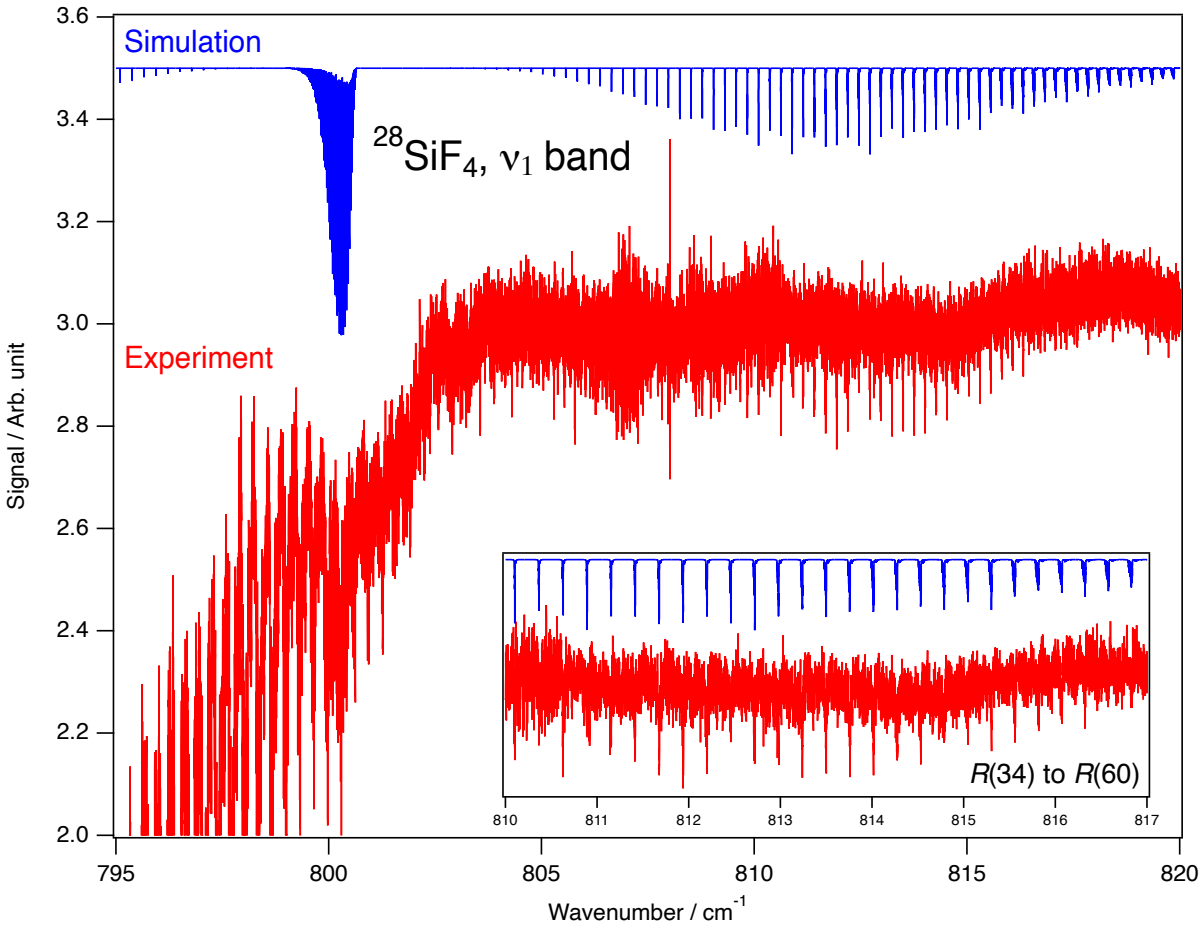

Figure 9: Mid-infrared transmission spectrum showing the weak ν_1 band, compared to the simulation. The very intense lines on the left correspond to the much stronger $2\nu_4$ overtone band. The insert shows part of the ν_1 R branch.

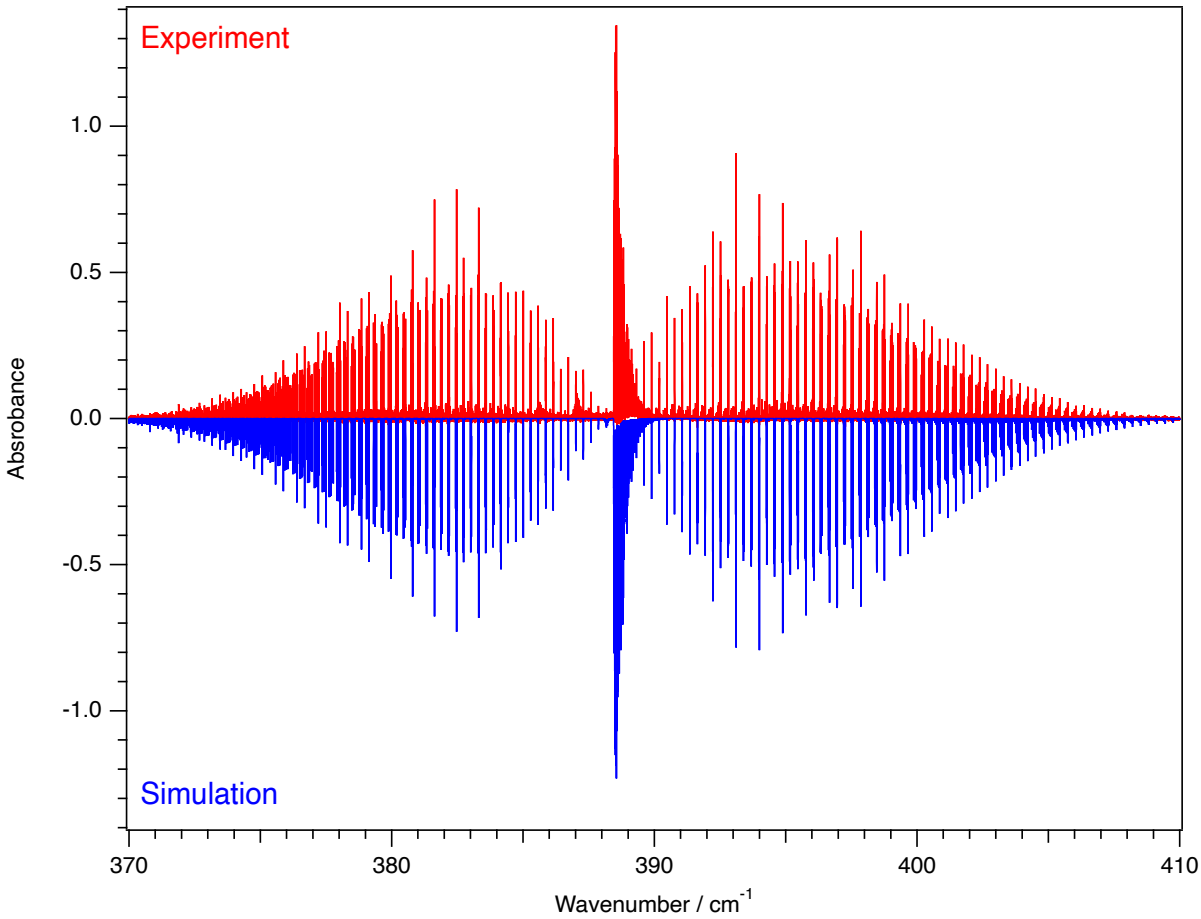

Figure 10: Experimental spectrum of the ν_4 band from Ref. [15] (at 160 K), compared to the simulation using the dipole moment derivative estimated in the present study.

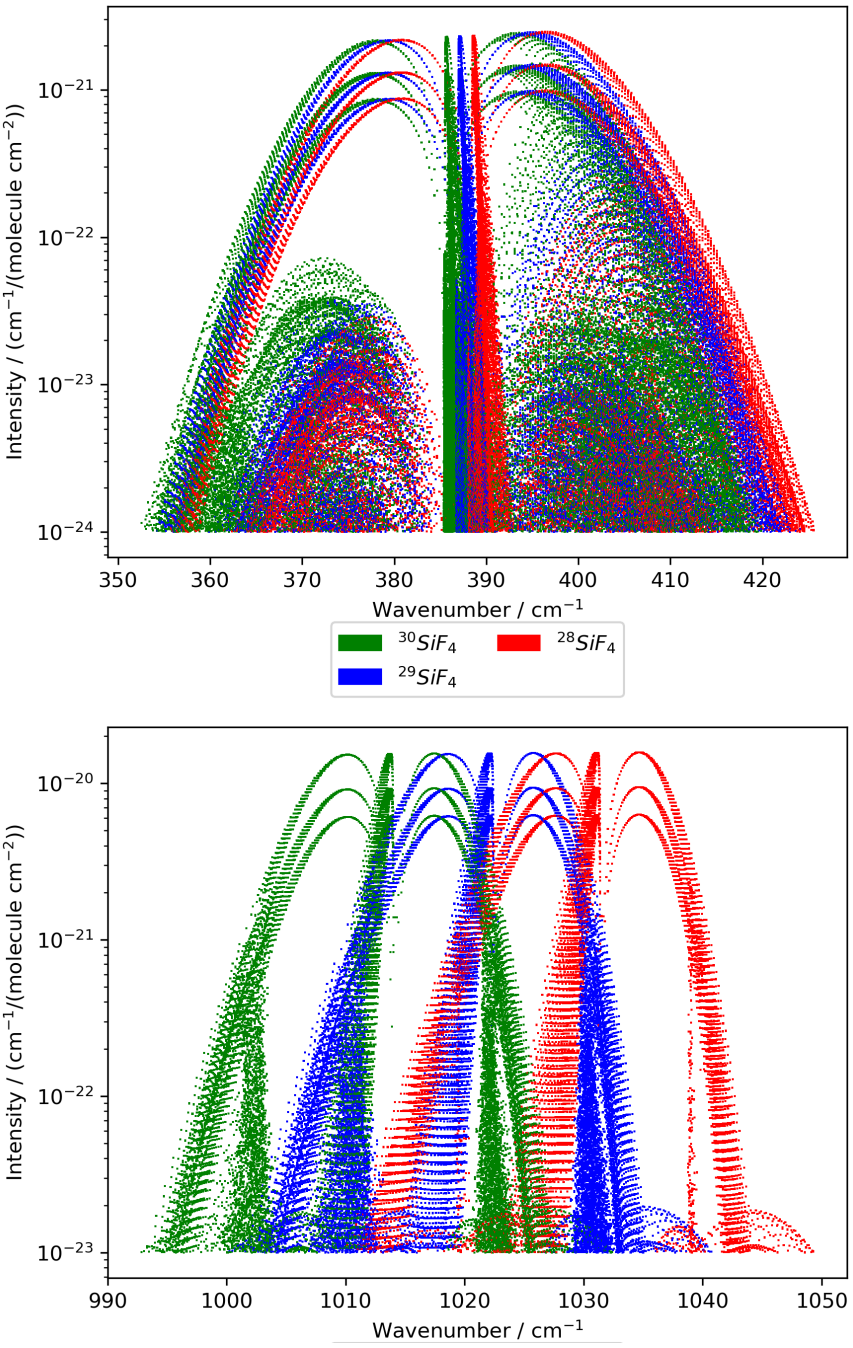

Figure 11: Extracted line by line list plotted on graphs as obtained from the TFSiCaSDa web page (`https://vamdc.icb.cnrs.fr/PHP/SiF4.php`). Both bands ν_3 and ν_4, corresponding to the entirety of the database, are represented on two separate panels, for the bending (top) and stretching (bottom) regions, for the three isotopologues. It should be noticed that the database does not include the isotopic abundance.

Tables

Table 1: Experimental conditions for the SiF_4 bands analyzed in this study.

Band	Pressure / mb × Path length / m	Temp / K	# averaged scans	Resolution / cm^{-1}	Beamsplitter/Detector/Cold filter
$\nu_4 - \nu_2$	14.9 × 93	163	576	0.002	6 μm Si-Mylar/Bolometer/0–350 cm^{-1}
$\nu_3 - \nu_1$	14.9 × 93	163	576	0.002	6 μm Si-Mylar/Bolometer/0–700 cm^{-1}
ν_2	0.44 × 93	163	360	0.001	6 μm Si-Mylar/Bolometer/0–700 cm^{-1}
$\nu_1 - \nu_4$	0.44 × 93	163	360	0.001	6 μm Si-Mylar/Bolometer/0–700 cm^{-1}
$2\nu_2$	14.9 × 93	163	576	0.002	6 μm Si-Mylar/Bolometer/0–700 cm^{-1}
$\nu_3 - \nu_4$	14.9 × 93	163	604	0.002	Ge-KBr/HgCdTe-4K/400–920 cm^{-1}
$\nu_2 + \nu_4$	14.9 × 93	163	604	0.002	Ge-KBr/HgCdTe-4K/400–920 cm^{-1}
ν_1	14.9 × 93	163	604	0.002	Ge-KBr/HgCdTe-4K/400–920 cm^{-1}

Table 2: Fitted effective Hamiltonian parameters for the fundamental levels fo $^{28}SiF_4$. Standard deviation is given in parentheses in the unit of the last two digits.

Level	$\Omega(K, nC)$	$\{\Gamma_v\}$ $\{\Gamma'_v\}$	Value / cm^{-1}		"Usual notation" [66, 67, 31] (when available)
GS	$2(0, 0A_1)$	$0000A_1$ $0000A_1$	1.3778055(14)	$\times 10^{-1}$	B_0
	$4(0, 0A_1)$	$0000A_1$ $0000A_1$	−4.138(11)	$\times 10^{-8}$	$-D_0$
	$4(4, 0A_1)$	$0000A_1$ $0000A_1$	−3.36051(68)	$\times 10^{-9}$	$-\left(\sqrt{15}/4\sqrt{2}\right) D_{0t}$
	$6(0, 0A_1)$	$0000A_1$ $0000A_1$	−2.1(2.6)	$\times 10^{-14}$	H_0
	$6(4, 0A_1)$	$0000A_1$ $0000A_1$	2.15(23)	$\times 10^{-15}$	$\left(3\sqrt{5}/16\sqrt{2}\right) H_{4t}$
	$6(6, 0A_1)$	$0000A_1$ $0000A_1$	3.54(49)	$\times 10^{-16}$	$-\left(\sqrt{231}/64\sqrt{2}\right) H_{6t}$
	$8(0, 0A_1)$	$0000A_1$ $0000A_1$	1.02(17)	$\times 10^{-17}$	$-L_0$
	$8(4, 0A_1)$	$0000A_1$ $0000A_1$	1.16(13)	$\times 10^{-19}$	$-\left(3\sqrt{15}/64\sqrt{2}\right) L_{4t}$
	$8(6, 0A_1)$	$0000A_1$ $0000A_1$	3.6(1.8)	$\times 10^{-20}$	$\left(3\sqrt{77}/256\sqrt{2}\right) L_{6t}$
	$8(8, 0A_1)$	$0000A_1$ $0000A_1$	−5.44(74)	$\times 10^{-20}$	$\left(1/32\sqrt{33}\right) L_{8t}$
$v_2 = 1$	$0(0, 0A_1)$	$0100E$ $0100E$	264.219525(32)		ν_2
	$2(0, 0A_1)$	$0100E$ $0100E$	−1.43084(28)	$\times 10^{-4}$	$B_2 - B_0$
	$2(2, 0E\ )$	$0100E$ $0100E$	−4.6789(22)	$\times 10^{-5}$	$\sqrt{3}\, b_2 + \left(24\sqrt{3}/7\right) C_6$
	$3(3, 0A_2)$	$0100E$ $0100E$	1.4181(26)	$\times 10^{-7}$	$(1/2)\, d_2$
	$4(0, 0A_1)$	$0100E$ $0100E$	3.911(56)	$\times 10^{-10}$	$-(D_2 - D_0)$
	$4(2, 0E\ )$	$0100E$ $0100E$	−1.009(28)	$\times 10^{-11}$	
	$4(4, 0A_1)$	$0100E$ $0100E$	3.535(86)	$\times 10^{-11}$	
	$4(4, 0E)$	$0100E$ $0100E$	−7.75(19)	$\times 10^{-11}$	
	$5(3, 0A_2)$	$0100E$ $0100E$	3.23(23)	$\times 10^{-13}$	
$v_4 = 1$	$0(0, 0A_1)$	$0001F_2$ $0001F_2$	388.433276(29)		ν_4
	$1(1, 0F_1)$	$0001F_2$ $0001F_2$	−2.75717(17)	$\times 10^{-2}$	$3\sqrt{2}\ B\zeta_4$ (ν_4 Coriolis)
	$2(0, 0A_1)$	$0001F_2$ $0001F_2$	1.68546(22)	$\times 10^{-4}$	$B_4 - B_0$
	$2(2, 0E\ )$	$0001F_2$ $0001F_2$	−1.17473(42)	$\times 10^{-4}$	$-(1/2)\alpha^4_{220} - 6\alpha^4_{224}$
	$2(2, 0F_2)$	$0001F_2$ $0001F_2$	5.5407(41)	$\times 10^{-5}$	$-(3/4)\alpha^4_{220} + 6\alpha^4_{224}$
	$3(1, 0F_1)$	$0001F_2$ $0001F_2$	−1.1536(25)	$\times 10^{-7}$	$-(3(\sqrt{3})/4(\sqrt{2})F^4_{110}$
	$3(3, 0F_1)$	$0001F_2$ $0001F_2$	−2.0263(12)	$\times 10^{-7}$	$(3/\sqrt{5}/2)F^4_{134}$
	$4(0, 0A_1)$	$0001F_2$ $0001F_2$	−2.639(35)	$\times 10^{-10}$	$-(D_4 - D_0)$
	$4(2, 0E\ )$	$0001F_2$ $0001F_2$	−1.842(37)	$\times 10^{-10}$	$\left(\sqrt{3}/8\right) G^4_{220} + \left(3\sqrt{3}/2\right) G^4_{224}$
	$4(2, 0F_2)$	$0001F_2$ $0001F_2$	7.88(42)	$\times 10^{-11}$	$\left(3\sqrt{3}/16\right) G^4_{220} - \left(3\sqrt{3}/2\right) G^4_{224}$
	$4(4, 0A_1)$	$0001F_2$ $0001F_2$	−1.292(76)	$\times 10^{-11}$	$\left(-3\sqrt{5}/4\sqrt{2}\right) (D_{4t} - D_{0t})$
	$4(4, 0E\ )$	$0001F_2$ $0001F_2$	8.21(30)	$\times 10^{-11}$	$\left(-3\sqrt{7}/2\right) G^4_{244} + \left(\sqrt{21}/2\sqrt{22}\right) G^4_{246}$
	$4(4, 0F_2)$	$0001F_2$ $0001F_2$	1.90(21)	$\times 10^{-11}$	$\left(-9\sqrt{7}/8\right) G^4_{244} - \left(\sqrt{21}/\sqrt{22}\right) G^4_{246}$
$v_1 = 1$	$0(0, 0A_1)$	$1000A_1$ $1000A_1$	800.66566(11)		ν_1
	$2(0, 0A_1)$	$1000A_1$ $1000A_1$	−1.5878(24)	$\times 10^{-4}$	$B_1 - B_0$
	$4(0, 0A_1)$	$1000A_1$ $1000A_1$	6.7(1.1)	$\times 10^{-10}$	$-(D_1 - D_0)$
	$4(4, 0A_1)$	$1000A_1$ $1000A_1$	4.70(70)	$\times 10^{-11}$	$\left(-\sqrt{15}/4\sqrt{2}\right) (D_{1t} - D_{0t})$
$v_3 = 1$	$0(0, 0A_1)$	$0010F_2$ $0010F_2$	1031.544438(65)		ν_3
	$1(1, 0F_1)$	$0010F_2$ $0010F_2$	3.1312443(17)	$\times 10^{-1}$	$3\sqrt{2}\ B\zeta_3$ (ν_3 Coriolis)
	$2(0, 0A_1)$	$0010F_2$ $0010F_2$	−2.9725(13)	$\times 10^{-4}$	$B_3 - B_0$
	$2(2, 0E\ )$	$0010F_2$ $0010F_2$	2.531816(74)	$\times 10^{-4}$	$-(1/2)\alpha^3_{220} - 6\alpha^3_{224}$
	$2(2, 0F_2)$	$0010F_2$ $0010F_2$	−0.996048(77)	$\times 10^{-4}$	$-(3/4)\alpha^3_{220} + 6\alpha^3_{224}$
	$3(1, 0F_1)$	$0010F_2$ $0010F_2$	1.0540(54)	$\times 10^{-7}$	$-(3(\sqrt{3})/4(\sqrt{2})F^3_{110}$
	$3(3, 0F_1)$	$0010F_2$ $0010F_2$	−2.46(14)	$\times 10^{-8}$	$(3/\sqrt{5}/2)F^3_{134}$
	$4(0, 0A_1)$	$0010F_2$ $0010F_2$	0.9(7.7)	$\times 10^{-11}$	$-(D_3 - D_0)$
	$4(2, 0E\ )$	$0010F_2$ $0010F_2$	−5.74(32)	$\times 10^{-9}$	$\left(\sqrt{3}/8\right) G^3_{220} + \left(3\sqrt{3}/2\right) G^3_{224}$
	$4(2, 0F_2)$	$0010F_2$ $0010F_2$	6.26(32)	$\times 10^{-9}$	$\left(3\sqrt{3}/16\right) G^3_{220} - \left(3\sqrt{3}/2\right) G^3_{224}$
	$4(4, 0A_1)$	$0010F_2$ $0010F_2$	8.71(60)	$\times 10^{-11}$	$\left(-3\sqrt{5}/4\sqrt{2}\right) (D_{3t} - D_{0t})$
	$4(4, 0E\ )$	$0010F_2$ $0010F_2$	9.20(48)	$\times 10^{-9}$	$\left(-3\sqrt{7}/2\right) G^3_{244} + \left(\sqrt{21}/2\sqrt{22}\right) G^3_{246}$
	$4(4, 0F_2)$	$0010F_2$ $0010F_2$	6.71(36)	$\times 10^{-9}$	$\left(-9\sqrt{7}/8\right) G^3_{244} - \left(\sqrt{21}/\sqrt{22}\right) G^3_{246}$
	$5(1, 0F_1)$	$0010F_2$ $0010F_2$	−9.89(40)	$\times 10^{-12}$	
	$5(3, 0F_1)$	$0010F_2$ $0010F_2$	−1.98(61)	$\times 10^{-12}$	
	$5(5, 0F_1)$	$0010F_2$ $0010F_2$	4.71(68)	$\times 10^{-12}$	
	$5(5, 1F_1)$	$0010F_2$ $0010F_2$	−9.13(57)	$\times 10^{-12}$	
	$6(0, 0A_1)$	$0010F_2$ $0010F_2$	−1.32(13)	$\times 10^{-13}$	$H_6 - H_0$
	$6(2, 0E\ )$	$0010F_2$ $0010F_2$	−1.462(98)	$\times 10^{-13}$	
	$6(2, 0F_2)$	$0010F_2$ $0010F_2$	1.44(10)	$\times 10^{-13}$	
	$6(4, 0A_1)$	$0010F_2$ $0010F_2$	−8.26(79)	$\times 10^{-15}$	
	$6(4, 0E\ )$	$0010F_2$ $0010F_2$	2.40(15)	$\times 10^{-13}$	
	$6(4, 0F_2)$	$0010F_2$ $0010F_2$	1.74(11)	$\times 10^{-13}$	
Nb. data			19432		
J_{max}			94		
Standard deviation			0.296		

Table 3: Rovibrational transitions in TFSiCaSDa.

Isotopologue	Transitions	# lines	Wavenumber range /cm^{-1}	Dipolar intensity range /(cm^{-1}/(molecule cm^{-2}))
	Scheme 1 (ν_3)			
$^{28}SiF_4$	$P_1 - P_0$	17 139	1010 – 1049	8×10^{-24} – 2×10^{-20}
$^{29}SiF_4$	$P_1 - P_0$	23 660	1000 – 1041	8×10^{-24} – 2×10^{-20}
$^{30}SiF_4$	$P_1 - P_0$	22 269	993 – 1032	8×10^{-24} – 2×10^{-20}
	Scheme 2 (ν_4)			
$^{28}SiF_4$	$P_1 - P_0$	44 564	356 – 426	8×10^{-25} – 2×10^{-21}
$^{29}SiF_4$	$P_1 - P_0$	45 113	354 – 424	8×10^{-25} – 2×10^{-21}
$^{30}SiF_4$	$P_1 - P_0$	57 656	353 – 421	8×10^{-25} – 2×10^{-21}
	Total	210 401		